An hybrid solver to compute a compressible model with dynamic estimation of the turbulent kinetic energy across shock waves

Sergey Gavrilyuk, Jean-Marc Hérard, Olivier Hurisse, Ali Toufaili

An hybrid solver to compute a compressible model with dynamic estimation of the turbulent kinetic energy across shock waves

Sergey Gavrilyuk[b,], Jean-Marc Hérard[a,], Olivier Hurisse[a,], Ali Toufaili[a,c,]

[a] *EDF R&D, 6 quai Watier, 78400 Chatou, France.*
[b] *IUSTI UMR CNRS 7343, Technopôle Château-Gombert, Marseille, France.*
[c] *I2M UMR CNRS 7373, Technopôle Château-Gombert, Marseille, France.*

Abstract

We propose in this paper a numerical strategy in order to compute a turbulence model for compressible flows, including a dynamical estimation of the jump of the turbulent kinetic energy across shock waves. The model is taken from [11], and the Finite Volume scheme applies for a specific interface Riemann solver. The whole procedure requires the detection of shock waves in unsteady flows.

Key words: Compressible turbulence models, entropy, shock waves, Riemann solvers.

*Corresponding author
Email addresses: sergey.gavrilyuk@univ-amu.fr (Sergey Gavrilyuk), jean-marc.herard@edf.fr (Jean-Marc Hérard), olivier.hurisse@edf.fr (Olivier Hurisse), ali.toufaili@edf.fr (Ali Toufaili)

Introduction

Many industrial applications require the computation of compressible turbulence models in order to obtain a relevant representation of the mean density, mean velocity, mean pressure and turbulent kinetic energy (for instance in the framework of combustion and aerodynamics). These models classically apply for Reynolds averaging technique and Favre decomposition [6, 7, 8], and closure laws for some correlations are mandatory. We refer for instance to [23, 22, 2, 20, 3, 9] which recall some basic useful models and closures, and also provide some properties and theoretical investigation of the latter.

This paper aims at defining a suitable algorithm for computing approximate solutions of a turbulence model for compressible flows, while retaining the dynamic model first introduced in [11]. It is actually the sequel of a recent work devoted to the analysis and the numerical approximation of solutions of the three-equation conservative model [10] for mass, momentum and energy. The latter model which is taken from [17], accounts for the turbulent kinetic energy K in a simple way, while setting:

$$K = \xi_0 \rho^{5/3}, \tag{1}$$

with $\xi_0 > 0$, together with the standard equation of state :

$$P = (\gamma - 1)\rho e. \tag{2}$$

The associated one-dimensional Riemann problem is investigated in [10], and it is shown that a Finite Volume scheme including approximate Riemann solvers enables to provide convergent approximations of solutions of

the model, even when shocks occur in the flow. Nonetheless, it may be argued that the closure law (1) does not account for turbulent entropy variations across a shock wave. This urges the introduction of a more relevant turbulence model which would enable to represent turbulent compressible flows with more accuracy. Moreover, even when restricting to smooth solutions, it is known that classical turbulence models also account for turbulent entropy variations in regular zones.

Thus we will present herein some way to account for K variations in the whole computational domain. For that purpose, we will first recall in section 1.2 the basic dynamic model proposed in [11], and detail the full parametrization of shock waves. This model will then be inserted in a set of PDEs that will govern the evolution of mass, momentum and total energy, together with the turbulent entropy $K\rho^{-5/3}$, hence providing the four unknowns ρ, P, U, K. This will be achieved in section 1.3. Afterwards, a Finite Volume scheme will be defined in section 2, that requires :

- the detection of the shock wave location in the unsteady flow at any time,
- the definition of a suitable interface Riemann-type solver in order to take turbulent entropy variations through shocks arising at an interface separating two neighboring mesh cells,
- a stable and consistent way to handle Dirac source terms occurring with shock patterns.

Eventually, some numerical results will be provided and discussed in section

3, and some conclusions will be drawn.

1. Governing equations

In this section, we present the steps used with the averaged Euler equations in order to derive a compressible model with dynamic estimation of the turbulent energy across a shock wave. This presentation consists in two different steps: (i) we start with the presentation of the global PDE formulation, (ii) we then move on to the presentation of the strategy used to estimate the jump of the turbulent entropy through a shock wave.

1.1. Global PDE formulation

The present model is an extension of the model presented in [17, 10] (the counterpart two- phase framework is presented in [18]), which is based on Euler equations for a compressible flow.

It includes three conservation laws corresponding to the mass, momentum and total energy balance. The main unknowns are: the mean density ρ, the mean pressure P (in the sense of Reynolds averaging) and the mean velocity u (in the sense of Favre averaging). A fourth equation accounting for the turbulent kinetic energy K describes the evolution of the turbulent entropy ξ:

$$\xi = K\rho^{-5/3}.$$

The set of PDEs which determine the evolution of variables ρ, u, P and ξ within the flow has the following form:

$$\begin{cases} \partial_t(\rho) + \partial_x(\rho u) = 0 \\ \partial_t(\rho u) + \partial_x\left(\rho u^2 + P + \dfrac{2K}{3}\right) = 0 \\ \partial_t(\rho E) + \partial_x\left(u\left(\rho E + P + \dfrac{2K}{3}\right)\right) = 0 \\ \partial_t(\rho\xi) + \partial_x(\rho u\xi) + M(x,t)\delta_{(x-\sigma t=0)} = 0 \end{cases} \tag{3}$$

by noting the mean total energy E:

$$\rho E = \rho e(P,\rho) + \frac{\rho u^2}{2} + K,$$

where e(P,ρ) is the mean specific internal energy given by user. We also note:

$$P^* = P + \frac{2}{3}K, \tag{4}$$

the modified pressure. The Dirac mass is $\delta_{(x-\sigma t=0)}$ located in $x = \sigma t$, $M(x,t)$ is the mass located at the shock position, and σ is the velocity of the shock wave.

Remark 1 (The special case $M(x,t) = 0$)
In the specific case where $M(x,t)$=0, the model associated with system (3) is conservative. We emphasize that (3) is hyperbolic (see **Appendix** A). Its real eigenvalues are:

$$\lambda_1 = u - \tilde{c}, \quad \lambda_{2,3} = u, \quad \lambda_4 = u + \tilde{c},$$

where the turbulent speed of density waves $\tilde{c}$ is given by:

$$\tilde{c}^2 = c^2 + \frac{10K}{9\rho} = c^2 + \frac{10}{9}\xi\rho^{2/3}.$$

When $M(x,t) = 0$, the Rankine-Hugoniot relations associated with model (3) are:

$$\begin{cases} -\sigma[\rho] + [\rho u] = 0, \\ -\sigma[\rho u] + \left[\rho u^2 + P + \dfrac{2K}{3}\right] = 0, \\ -\sigma[\rho E] + \left[u\left(\rho E + P + \dfrac{2K}{3}\right)\right] = 0 \\ -\sigma[\rho\xi] + [\rho u\xi] = 0 \end{cases} \tag{5}$$

The first relation gives us:

$$[\rho v] = 0, \quad with \quad v = u - \sigma.$$

The fourth relation can be written in the following form:

$$[\rho v\xi] = 0 \Longrightarrow \rho v[\xi] = 0$$

Through a shock wave (GNL field), we have $\rho v \neq 0$, thus $[\xi]_L^R$=0 where L (R) respectively denote the variables ahead (behind) the shock wave.

Besides, we note that ξ is a Riemann invariant in GNL waves associated with λ_1 and λ_4. Hence, we deduce that ξ remains constant in GNL waves (shock or rarefraction). ■

However, it is usually argued that the 'closure' $[\xi]_L^R$=0 through a shock wave (or $M(x,t) = 0$) is not totally realistic. Focusing for instance on hydrogen explosion, an accurate prediction of shock waves is mandatory, and thus a relevant (non zero) definition of the mass $M(x,t)$ is required.

This is discussed in the following section, while **Appendix** D gives some

possible reformulation of the governing set of PDE when a sole shock wave occusion in the fluid flow.

1.2. Estimation of the turbulent entropy jump through a shock wave

We will consider in the sequel the model which has been proposed in [11]. The latter reference proposes a methodology to evaluate the jump of turbulent entropy through shock waves.

1.2.1. Estimating $M(x,t)$

In the sequel, we will consider the following turbulent perfect gas EOS:

$$P = (\gamma - 1)\rho e.$$

with $\gamma > 1$.

For a given shock wave propagating at speed σ, we note the variables on the right side of the shock with the index 'R', and the variables of the left side of the shock with index '2' (thus focusing on the wave associated with $u + \tilde{c}$). The following Rankine-Hugoniot relations for the conservation of mass, momentum and energy can be easily obtained using (6)

$$\begin{cases} [\rho(u-\sigma)]_2^R = 0 \\ m^2[\tau]_2^R + [P^*]_2^R = 0 \\ [e + K\tau]_2^R + \bar{P}^*_{R,2}[\tau]_2^R = 0 \end{cases} \tag{6}$$

with $m = \rho_R(u_R - \sigma)$, and for any quantity ϕ: $\bar{\phi}_{a,b} = \frac{\phi_a + \phi_b}{2}$, $[\phi]_b^a = \phi_a - \phi_b$.

The fourth equation in (3) enables to get:

$$-\sigma[\rho\xi]_2^R + [\rho u\xi]_2^R + M_0 = 0 \Longrightarrow m[\xi]_2^R + M_0 = 0 \tag{7}$$

In order to determine the intermediate state '2' from the state 'R', and therefore to find the value of M_0, one more relation is needed.

- The second and the third equation of (6) are written in the form:

$$\begin{cases} P_2^* - P_R^* - m^2(\tau_R - \tau_2) = 0 \\ P_R^*(\beta\tau_R - \tau_2) - P_2^*(\beta\tau_2 - \tau_R) + 2\xi_R\tau_R^{-2/3}\alpha - 2\xi_2\tau_2^{-2/3}\alpha = 0 \end{cases} \tag{8}$$

  where:

$$\alpha = \frac{(\gamma - 5/3)}{(\gamma - 1)},$$

  and

$$\beta = \frac{(\gamma + 1)}{(\gamma - 1)}.$$

  System (8) admits 2 equations with 3 unknowns: P_2^*, τ_2 and ξ_2.

  The first relation in (8) determines the Rayleigh line, and we call the function $H(\tau_2, P_2^*, \xi_2)$ the Hugoniot function of the turbulent gas flow defined by second relation in (8) :

$$H(\tau_2, P_2^*, \xi_2) = P_R^*(\beta\tau_R - \tau_2) - P_2^*(\beta\tau_2 - \tau_R) + 2\xi_R\tau_R^{-2/3}\alpha - 2\xi_2\tau_2^{-2/3}\alpha \tag{9}$$

- **The additional relation is given by following** [11], the tangent of the Rayleigh line to the curve H in the plane (τ_2, P_2^*) with ξ_2 fixed, gives us the additional relation. We rewrite this constraint by solving the following equation:

$$\frac{\partial H}{\partial \tau}|_{(P^*,\xi)} d\tau|_\xi + \frac{\partial H}{\partial P^*}|_{(\tau,\xi)} dP^*|_\xi = 0, \tag{10}$$

  which gives us the following equation:

$$\frac{4}{3}\xi_2\tau_2^{-5/3}\alpha = P_R^* + P_2^*\beta + m^2\tau_R - m^2\tau_2\beta. \tag{11}$$

For a given value of $(\tau, u, P, \xi)_R$ and σ, we have to find 5 unknowns $(\tau, u, P, \xi)_2$ and M_0 solution of (6), (7) and (11).

1.2.2. Positivity conditions

We investigate now the positivity conditions pertaining to ξ_2 (or equivalently K_2). Actually, since ξ_2 must have a positive value, conditions pertaining to the jump of τ will appear when crossing the shock, depending on the value of the parameter γ .

We denote by:

$$\mathcal{A} = P_R^* + P_2^*\beta + m^2\tau_R - m^2\tau_2\beta,$$

the right hand side of equation (11). Assuming that $\tau_2 > 0$ therefore $\xi_2 > 0$, then $\mathcal{A}$ will take the sign of (γ-5/3) (linked to α).

- **case** $\gamma < 5/3$:

  Since (γ-5/3) has a negative sign, then $\mathcal{A}$ must be negative for ξ_2 to remain positive. Using the first relation of system (8) and the definition of P^* (4), we reformulate $\mathcal{A}$ in the following form :

  $$\mathcal{A} = \tilde{c_R}^2 + \frac{2}{3}K_R\tau_R(\gamma - 5/3) - m^2\left((\gamma+1)\tau_2\tau_R - \gamma\tau_R^2\right).$$

  When A <0, it is necessary that:

  $$m^2\left((\gamma+1)\tau_2\tau_R - \gamma\tau_R^2\right) > \tilde{c_R}^2 + \frac{2}{3}K_R\tau_R(\gamma - 5/3). \qquad (12)$$

  Using Lax inequality:

  $$\sigma > \lambda_4(W_R), \qquad (13)$$

we deduce from (13) that:

$$\tilde{c_R}^2 + \frac{2}{3} K_R \tau_R (\gamma - 5/3) > 0.$$

Owing to $m^2 > 0$, a condition involving the jump $[\tau]_2^R$ appears, which is:

$$(\gamma + 1)\tau_2 \tau_R - \gamma \tau_R^2 > 0,$$

and eventually ($\tau_R > 0$):

$$\tau_2 > \frac{\gamma}{(\gamma + 1)} \tau_R. \tag{14}$$

- **case** $\gamma > 5/3$:

  in the case where the shock is of low amplitude (i.e $\tau_R \approx \tau_2$) and the turbulence is weak (i.e $K_R << 1$), $\mathcal{A}$ writes:

$$\mathcal{A} = P_R(1 + \beta) + m^2 \tau_R (1 - \beta) = (c_R^2 - (u_R - \sigma)^2) \frac{1}{\tau_R}.$$

  Thanks to the Lax inequality (13), which gives:

$$\sigma > u_R + \tilde{c_R} > u_R + c_R,$$

  we get that:

$$\sigma - u_R > c_R > 0,$$

  Thus $\mathcal{A}$ must be negative. However this is in contradiction with (11)

$$\frac{4}{3} \xi_2 \tau_2^{-5/3} \alpha = \mathcal{A},$$

  when $\gamma > 5/3$, that is: $\alpha > 0$.

  Remark 2 (case $\gamma > 5/3$ with $\tau_R \neq \tau_2$ and $K_R >> 1$)
  In this case we will not explicitly give the positivity conditions, because in an extension of this case ($\tau_R \approx \tau_2$ and $K_R << 1$) we have found a contradiction, therefore we do not take this case into account and we just focus on the case where $\gamma < 5/3$. ■

1.2.3. Final form of M(x,t)

Using the additional relation (11) and system (8), simple calculations lead to solve a second order polynomial equation in τ_2, G(τ_2)=0, where:

$$G(\tau_2) = 2m^2\beta\tau_2^2 - \frac{5\gamma}{2(\gamma-1)}(m^2\tau_R + P_R^*)\tau_2 + P_R^*\tau_R\frac{\gamma}{\gamma-1} + \frac{1}{2}m^2\tau_R + \xi_R\tau_R^{-2/3}\alpha. \tag{15}$$

Equation (15) admits a unique solution under the two constraints:

$$\tau_2 < \tau_R \quad , \quad \tau_2 > \frac{\gamma}{(\gamma+1)}\tau_R. \tag{16}$$

Once τ_2 has been obtained by solving G(τ_2)=0, the first equation in (6) gives u_2, the second one gives P_2^*, the third one gives:

$$[\frac{P^*\tau}{(\gamma-1)} + \alpha\xi\tau^{-2/3}]_2^R + P_{2,R}^{\bar{*}}[\tau]_2^R = 0 \tag{17}$$

which in turn provides ξ_2. Then the jump $[\xi]_2^R$ is known, and we can calculate M_0 by equation (7):

$$M_0 = -m[\xi]_2^R.$$

Of course a similar approach is used across the shock wave associated with $u - \tilde{c}$.

Remark 3 The Lax criterion applied to our system states that for an admissible shock wave with a velocity σ we have for a $(u + \tilde{c})$-shock:

$$\lambda_4(W_2) = u_2 + \tilde{c_2} > \sigma > \lambda_4(W_R) = u_R + \tilde{c_R} \tag{18}$$

In fact, we have:

$$\sigma - u_2 - \tilde{c_2} = m^2\tau_2^2 - \gamma P_R^*\tau_2 - \gamma\tau_R\tau_2 + \gamma m^2\tau_2^2 + \frac{2}{3}\xi_2\tau_2^{-2/3}(\gamma - \frac{5}{3}),$$

using the first and second equations of (6). By replacing ξ_2 by its value given by equation (11), we find that:

$$\sigma - u_2 - \tilde{c_2} = 0,$$

which means that the first inequality in (18) is reached. ■

2. Numerical method

In this part we will introduce a numerical method in order to cope with the compressible turbulence model (3) described in the previous part. The method consists in adapting a hybrid solver to compute approximate solutions of the problem. This hybrid solver consists in two solvers: a classical approximate interface Riemann solver when no shock wave is detected, and a specific interface solver dedicated to the interface where a shock wave has been detected. We will call it the modified approximate Riemann solver 'MARS'.

For this, we use a classical Finite Volume formulation in a 1D domain. The computational domain on segment [a,b] is subdivided into cells I_i, where $x_{i+1/2}$ represents the cell interface between cells I_i and I_{i+1}, and x_i represents the cell center. We define Δt^n the time step at time t^n and Δx_i the length of I_i such that: $t^{n+1} = t^n + \Delta t^n$ and $\Delta x_i = x_{i+1/2} - x_{i-1/2}$.

In the sequel, we will define the modified solver, more particularly the interface solver applied when a shock wave is detected on an interface. Concerning the classical approximate Riemann solver we will not detail it, because it is

already known in the literature, the reader is referred to [14, 13, 24] for more details.

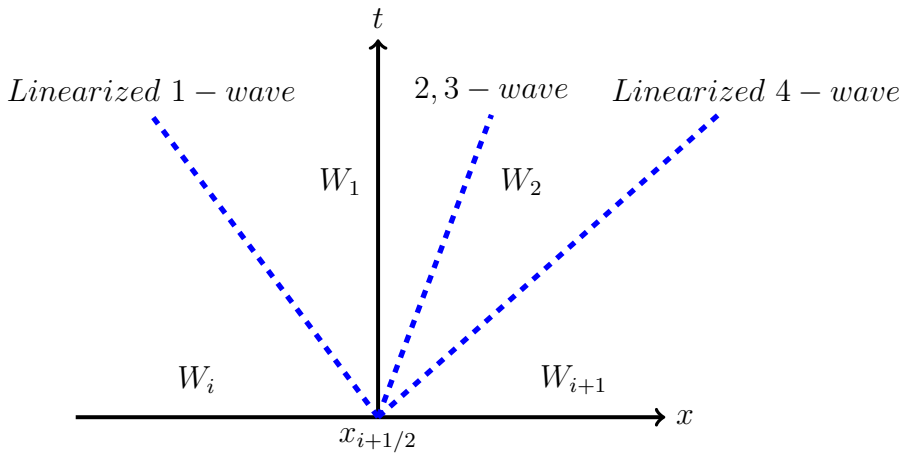

Figure 1: Classical linearized interface solver at the interface $(i+\frac{1}{2})$ when no shock has been detected.

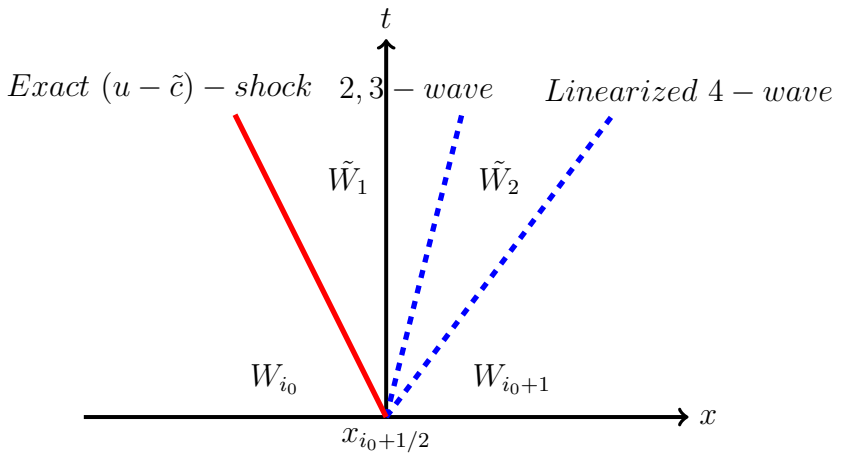

Figure 2: Modified interface solver 'MARS', if a (u-$\tilde{c}$)-shock is detected at the interface $(i_0+\frac{1}{2})$.

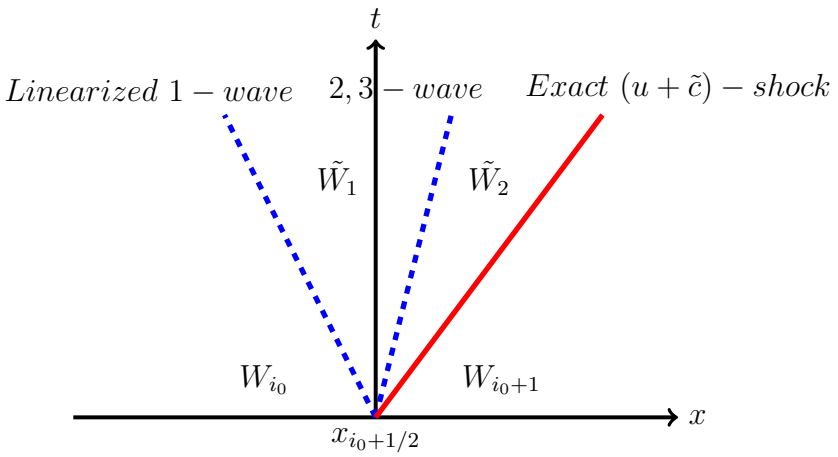

Figure 3: Modified interface solver 'MARS', if a (u-$\tilde{c}$)-shock is detected at the interface $(i_0 + \frac{1}{2})$.

2.1. Shock detector

In order to define properly the modified interface Riemann-type solver on the interface where a shock wave has been detected, a practical technique of detection of shock waves is needed. There are some methods proposed in the literature to detect shock waves (see [19, 25] for instance for steady patterns), however only few focus on the unsteady framework, as pointed out in the conclusion of paper [25]. Thus, a different strategy will be introduced in the sequel, which basically relies on properties of the solution of the one-dimensional Riemann problem, on the entropy inequality and on associated Lax inequalities (see [21]).

For an interface $'i + \frac{1}{2}'$ separating the two cells i and $i+1$, we define the quantity $g_{i,i+1}$ as follows:

$$g^n_{i,i+1} = -\sigma_{i+1/2}[\eta^n]^{i+1}_i + [f^n_\eta]^{i+1}_i, \tag{19}$$

where (η, f_η) denotes the entropy-entropy flux pair, with $\eta = -\rho s$ and $f_\eta = u\eta$. The estimation of the shock velocity is made on the basis of the mass balance:

$$\sigma_{i+1/2} = \frac{[(\rho u)^n]_i^{i+1}}{[\rho^n]_i^{i+1}}. \tag{20}$$

Actually, for a discontinuity between the cells 'i' and 'i+1' travelling at speed $\sigma_{i+\frac{1}{2}}$, we have the following inequality:

$$-\sigma_{i+1/2}[\eta^n]_i^{i+1} + [f_\eta^n]_i^{i+1} < 0. \tag{21}$$

The use of jump relations (6)-(7) makes it possible to give a simple form of the quantity g:

$$g_{i,i+1}^n = \frac{\rho_i^n \rho_{i+1}^n [u^n]_i^{i+1} [s^n]_i^{i+1}}{[\rho^n]_i^{i+1}}.$$

We can deduce that if $g_{i,i+1}^n < 0$ then we have detected a discontinuity zone.

Though redundant, we also enforce the test:

$$[u^n]_i^{i+1} < 0,$$

where $[u^n]_i^{i+1}$ is expected to be o(1) through shock waves (unlike through 'discrete' contact discontinuities where $[u]_i^{i+1} \approx o(h)$).

Finally the test will be in the following form:

if $g_{i,i+1}^n < 0$ and $[u^n]_i^{i+1} < 0$, *then a shock wave is detected on the interface in* $i + \dfrac{1}{2}$

Once we have detected the interfaces with occurence of a shock wave, it remains to know whether it is a (u-$\tilde{c}$)-shock or a (u+$\tilde{c}$)-shock wave. The definition of shock waves in the sense of Lax will be used to distinguish them:

- if $u_i - \tilde{c_i} > \sigma_{i+1/2} > u_{i+1} - \tilde{c}_{i+1}$, then a $(u - \tilde{c})$-shock wave is detected on the interface in $'i + \frac{1}{2}'$
- if $u_i + \tilde{c_i} > \sigma_{i+1/2} > u_{i+1} + \tilde{c}_{i+1}$, then a $(u + \tilde{c})$-shock wave is detected on the interface in $'i + \frac{1}{2}'$

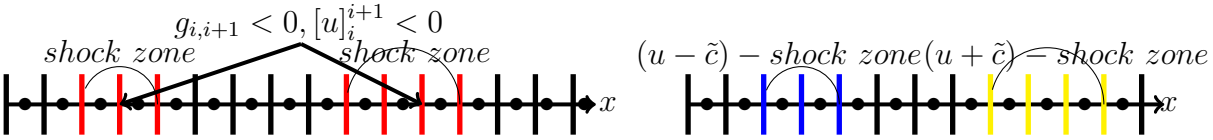

Figure 4: Two different steps of the shock detector. Step 1 (left) shock zone detection, step 2 (right) (u-$\tilde{c}$)-shock or (u+$\tilde{c}$)-shock identification. Interface colors: shock zone (red), 1-shock (blue), 3-shock (yellow) and for other waves types (black)

In practice, most of the time the shock zone involves more than a sole interface, as depicted in figure (4).

2.2. Modified Approximate Riemann Solver when a shock occurs 'MARS'

This section describes the numerical resolution of the Riemann problem associated with a shock detected on the interface. More precisely we want to evaluate the numerical flux $F^{MARS}_{i_0+\frac{1}{2}}$ associated with the shock wave at interface $i_0 + \frac{1}{2}$. For the detection step, we assume that shock speeds have been estimated. Moreover the mass M_0 is given here.

In the following, we consider the general case $\mathbf{M \neq 0}$. In order to simplify the presentation of the modified solver, we focus on the case of an effective shock in the 4-wave (i.e. when a (u+$\tilde{c}$)-shock appears).

First of all, we recall that (see [10], or **Appendix** A) the eigenvalues of system (3) are:

$$\lambda_1(W) = u - \tilde{c}, \quad \lambda_{2,3}(W) = u, \quad \lambda_4(W) = u + \tilde{c}$$

The associated eigenvectors are respectively:

$$r_1(W) = (\rho, -\tilde{c}, \rho\tilde{c}^2, 0) \quad , \quad r_2(W) = (1, 0, 0, 0)$$

$$r_3(W) = (0, 0, 0, 1) \quad , \quad r_4(W) = (\rho, \tilde{c}, \rho\tilde{c}^2, 0)$$

where

$$W = (\rho, u, P^*, \xi), \tag{22}$$

is the set of variables considered here.

The double wave associated with $\lambda_{2,3}$ is linearly degenerate (LD), and r_2 and r_3 are independent. The variables (u, P^*) are the Riemann invariants in this double wave.

The wave configuration retained for the simplified solver at the interface is depicted in figure 5.

We note that:

$$W_1 - W_i = \mu_{i+\frac{1}{2}} \tilde{r}_1, \tag{23}$$

with $\tilde{r}_1 = (\bar{\rho}, -\bar{\tilde{c}}, \bar{\rho\tilde{c}^2}, 0)_{i+\frac{1}{2}}$, where $\bar{a} = \frac{a_{i+1}+a_i}{2}$ ($\mu_{i+\frac{1}{2}}$ will be given in step 3).

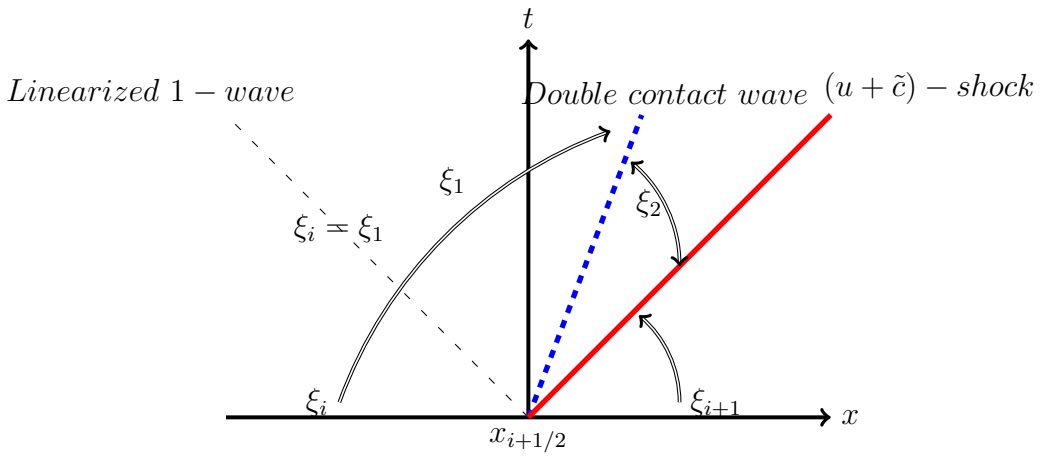

Figure 5: Partial solution of the Riemann problem in terms of ξ. Intermediate states noted '1','2'

Concerning the wave associated with λ_4, we assume that it is a shock wave. The jump relations associated with this wave are as follows :

$$\begin{cases} \rho_R(u_R - \sigma) = \rho_2(u_2 - \sigma) = m \\ m^2[\tau]_2^R + [P^*]_2^R = 0 \\ [e + K\tau]_2^R + \bar{P}^*_{R,2}[\tau]_2^R = 0 \\ m[\xi]_2^R + M_0 = 0 \end{cases} \tag{24}$$

where W_R=W_{i+1}.

The shock speed $\sigma_{i+1/2}$ is known numerically on the interface thanks to the detection stage (20). We recall that ξ_2 is known since M_0 is known, according to the formula proposed in section 1.2. We can then deduce from the jump relations (24) the three unknowns $(\rho, u, P)_2$ for the intermediate state '2'.

At this stage, we can propose a modified approximate Riemann solver 'MARS'

adapted to the specific configuration of a (u+$\tilde{c}$)-shock wave. We calculate in three steps which are::

1. Use of the jump relation through 4-wave.
2. Exact connection through the double contact wave $\lambda_{2,3} = u$.
3. Connection between state 'L' and '1' through linearized 1-wave.

Remark 4 The second and the third step of modified solver are the same as for the classical solver VFRoe-ncv [4]. ■

We recall that:

$$P = (\gamma -)\rho e. \tag{25}$$

• **Step 1((u+$\tilde{c}$)-shock)**: The jump relations (24) give us:

$$P_2^*(\tau_2) = P_R^* - m^2(\tau_R - \tau_2), \tag{26}$$

$$u_2(\tau_2) = \sigma_{i+1/2} + m\tau_2, \tag{27}$$

with

$$\sigma_{i+1/2} = \frac{[\rho u]_i^{i+1}}{[\rho]_i^{i+1}} = \bar{u} + \bar{\rho}\frac{[u]_i^{i+1}}{[\rho]_i^{i+1}}. \tag{28}$$

Using relations (27) (26), and third relation of (24), we have to solve a nonlinear scalar equation of unknown τ_2:

$$\gamma(P_2^*(\tau_2) + P_R^*)(\tau_R - \tau_2) + (\tau_R + \tau_2)(P_R^* - P_2^*(\tau_2)) + 2(\gamma - \frac{5}{3})[K\tau]_2^R = 0. \tag{29}$$

From a pratical point of view, the nonlinear equation (29) is solved using the dichotomy method, thus $\rho_2 = \frac{1}{\tau_2}$ is known.

Using (27) (respectively (26)), we get the intermediate speed u_2 (the intermediate pressure P_2^*). The calculation of the intermediate state '2' guarantees that :

$$[\rho]_2^R[P^*]_2^R > 0 \text{ and } \ [u]_2^R < 0. \tag{30}$$

• **Step 2 (double contact wave):** Knowing that the Riemann invariants associated with the contact wave are (u, P^*), we set:

$$u_1 = u_2 \ \text{ and } P_1^* = P_2^*. \tag{31}$$

• **Step 3 (Linearized 1- wave):** u_1 and P_1^* are now known, thus using (23) we obtain:

$$\rho_1 = \rho_L + \frac{[P^*]_L^1}{\tilde{c_{L,R}}}. \tag{32}$$

This guarantees that:

$$[\rho]_L^1[P^*]_L^1 > 0. \tag{33}$$

The modified interface solver is now fully defined.The intermediate states are defined as follows:

$$W_k^{MARS} = (\rho_k, u_k, P_k^*, \xi_k), \ k = 1, 2. \tag{34}$$

and then the numerical flux $F_{i_0+1/2}^{MARS}$ is defined through (37), (38) and (40). ■

Now we can move on to the presentation of the finite volume scheme that is based on these two Riemann solvers.

Remark 5 Even if $M_0 = 0$, the 'MARS' solver is not strictly the VFRoe-ncv solver [4, 10]. ■

2.3. Global solver and numerical scheme

In this section, we present a finite volume scheme [5], for the numerical resolution of the following system of equations:

$$\begin{cases} \partial_t(\rho) + \partial_x(\rho u) = 0 \\ \partial_t(\rho u) + \partial_x\left(\rho u^2 + P + \dfrac{2K}{3}\right) = 0 \\ \partial_t(\rho E) + \partial_x\left(u\left(\rho E + P + \dfrac{2K}{3}\right)\right) = 0 \\ \partial_t(\rho\xi) + \partial_x(\rho u\xi) + M_0\delta_{(x-\sigma t=0)} = 0 \end{cases} \tag{35}$$

where $M_0 = 0$, or M_0 given by section (1.2).

The numerical scheme reads :

$$\Delta x_i(Z_i^{n+1} - Z_i^n) + \Delta t(\mathcal{F}_{i+\frac{1}{2}}^n - \mathcal{F}_{i-\frac{1}{2}}^n) + \Delta t B_i^n = 0, \tag{36}$$

with $Z = (\rho, \rho u, \rho E, \rho\xi)$, $B_i = (0, 0, 0, M_i)$, and:

$$\mathcal{F}_{i+\frac{1}{2}}^n = \begin{cases} \mathcal{F}_{i+\frac{1}{2}}^{lnd} = F(Z(W_{lnd}^*(W_i^n, W_{i+1}^n)) \text{ when no shock wave has been detected,} \\ \\ \mathcal{F}_{i+\frac{1}{2}}^{MARS} = F(Z(W_{MARS}^*(W_i^n, W_{i+1}^n)) \text{ if a shock wave has been detected,} \end{cases} \tag{37}$$

where:

$$F(Z) = (\rho u, \rho u^2 + P^*, u(\rho E + P^*), \rho u\xi). \tag{38}$$

The solution $W_{lnd}^*(W_L, W_R)$ of the approximate Riemann problem, is found with the linearized solver VFRoe-ncv (see [4, 10]). When no shock wave is

detected on the interface, the solution of the Riemann problem is given by :

$$W^*_{lnd}(W_L, W_R) = \begin{cases} W_L \ \text{ if } \ \bar{\lambda}_1 \geq 0; \\ \\ W_1^{lnd} \ \text{ if } \ \bar{\lambda}_1 < 0 \text{ and } \bar{\lambda}_{2,3} \geq 0; \\ \\ W_2^{lnd} \ \text{ if } \ \bar{\lambda}_{2,3} < 0 \text{ and } \bar{\lambda}_3 \geq 0; \\ \\ W_R \ \text{ if } \ \bar{\lambda}_4 < 0; \end{cases} \tag{39}$$

For more details about the solution W^*_{lnd}, the reader is referred to **Appendix** B.

The solution $W^*_{MARS}(W_L, W_R)$ of the approximate Riemann problem, is found with the modified interface solver 'MARS'. If a shock wave has been detected on the interface, the solution of the Riemann problem is given thus by :

$$W^*_{MARS}(W_L, W_R) = \begin{cases} W_L \ \text{ if } \ \lambda_1 \geq 0; \\ \\ W_1^{MARS} \ \text{ if } \ \lambda_1 < 0 \text{ and } \lambda_{2,3} \geq 0; \\ \\ W_2^{MARS} \ \text{ if } \ \lambda_{2,3} < 0 \text{ and } \lambda_3 \geq 0; \\ \\ W_R \ \text{ if } \ \lambda_4 < 0; \end{cases} \tag{40}$$

where W_1^{MARS}, W_2^{MARS} are the 2 intermediate states, calculated in the section 2.2.

M_i^n is a contribution in cell i to the global jump of turbulent entropy M_0. It appears when a shock wave has been detected locally. In order to guarantee that $\sum_{i=1}^{N} M_i^n = M_0$ (recall that N is the total number of cells in the domain and M_0 is the global jump of turbulent entropy to be imposed on shock wave), the calculation of M_i is done as follows :

- We set $M_i^n = 0$, $\forall$ i $\in$ N, at each time step time n .

  - Loop 1 : if a shock is detected at interface i+1/2 :

$$\begin{aligned} &1.\ \chi_{i+\frac{1}{2}}^n = |\rho_{i+1}^n - \rho_i^n|, \\ &2.\ Sum^n = \sum_{i=1}^{N} \chi_{i+\frac{1}{2}}^n. \end{aligned} \tag{41}$$

  - Loop 2 : if a shock is detected at interface i+1/2:

$$1.\ \tilde{\chi}_{i+\frac{1}{2}}^n = \frac{\chi_{i+\frac{1}{2}}^n}{Sum^n}, \tag{42}$$

$$2.\ \begin{cases} \text{si} \quad \sigma_{i+1/2} < 0 \rightarrow M_i^n = M_i^n + \tilde{\chi}_{i+1/2}^n * M_0 \\ \\ \text{si} \quad \sigma_{i+1/2} > 0 \rightarrow M_{i+1}^n = M_{i+1}^n + \tilde{\chi}_{i+1/2}^n * M_0 \end{cases}$$

Moreover, Δt^n and Δx_i are linked by the Courant-Friedrichs-Levy (CFL) following condition :

$$\frac{\Delta t^n}{\Delta x_i} max(|\lambda_j|_{j=1,2,3,4}) < 1,$$

in scheme (36).

3. Numerical Results

We present now some numerical results obtained for the model and scheme detailed in the previous sections. We focus here on test cases involving shock waves. The test cases provide a comparison between the exact solution and the approximate solution and make it possible to obtain a numerical convergence curve, which gives the error in L1 norm. The profiles of the approximate solutions are presented at a given final time for the density ρ, velocity u, pressure P, modified pressure P^*, and the turbulent entropy ξ.

All the computations are performed for a given value of $CFL = 0.5$. Moreover, in all the tests below, we have considered the perfect gas EOS:

$$P = (\gamma - 1)\rho e,$$

where the constant γ is equal to $\frac{7}{5}$. The computational domain is $[0, 1]$ and the initial discontinuity separating states W_L and W_R is located at x= 0.5. The domain $[0, 1]$ is discretized using uniform cells, $\Delta x_i = \Delta x$, and the number of cells varies from 200 up to $2\times\ 10^5$ cells.

3.1. Test 1: Double shock wave ($\xi = \xi_0$)

The first test case is a double non-symmetrical shock with a mass $M_0 = 0$. This case is used to test the modified interface solver, on the basis of the pure conservative system (turbulence entropy is constant), and to compare the results with classical solver [10].

This case test is taken from [10]. The initial conditions of the Riemann

problem to be solved are given below:

$$(\rho_L, u_L, P_L, \xi_L) = (1, 650, 10^6, 10^4)$$

$$(\rho_R, u_R, P_R, \xi_R) = (1, -687.545913, 98007.273140, 10^4)$$

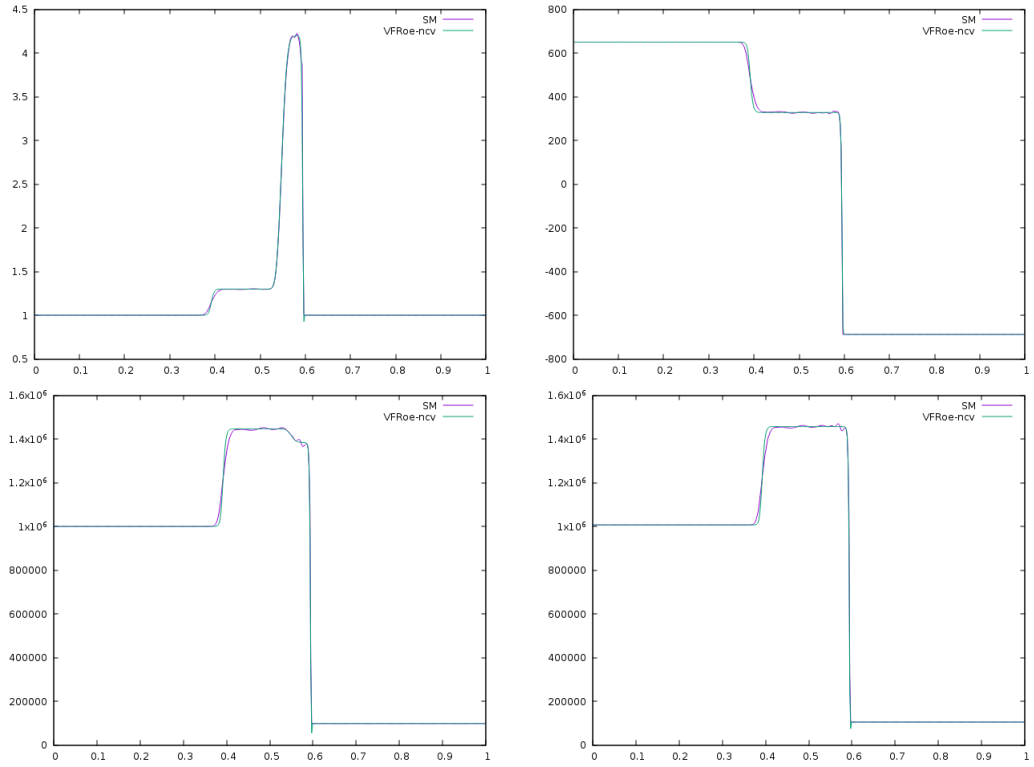

Figure 6: Double-shock wave test case. Density (top left), velocity (top right), pressure (bottom left) and P^* (bottom right). Comparison between the modified interface solver (green) and the VFRoe-ncv solution (purple) at $t = 144 \times 10^{-3}$ s, $CFL = 0.5$, 500 cells.

Figure 6 shows qualitative comparisons between the approximate solutions calculated with the modified interface solver 'MARS' and the linearized solver VFRoe-ncv for a mesh containing 500 cells. Figure 7 shows the convergence

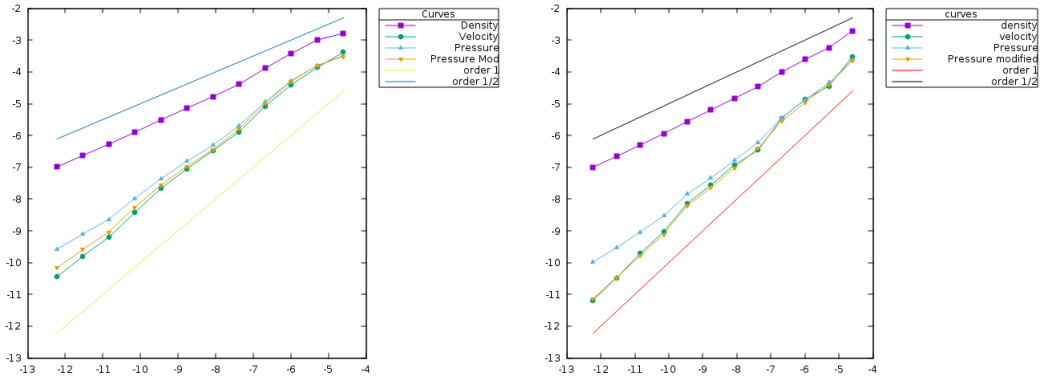

Figure 7: Double-shock wave test case. Convergence curves, with modified interafce solver (left), VFRoe-ncv (right): logarithm of the relative L1-error versus the logarithm of the mesh size with uniform meshes containing from 200 to 200000 cells. The error is plotted for variables, ρ, u, P and P^*.

curves, with the two solvers ('MARS' and VFRoe-ncv), for the set of variables $\{\rho$, u, P, $P^*\}$, and for $\xi_L = \xi_R = 10^4$, M_0=0.

First of all, the behavior of 'MARS' near the 3-shock wave around $x = 0.6$ is steep but oscillating (see figure 6). The error curve for VFRoe-ncv and 'MARS' on P and ρ is comparable but a little better for VFRoe-ncv on u and P^*. The error (for 'MARS') varies as $\approx h^1$ for variables u and P^* on fine meshes, and as $h^{1/2}$ for ρ and P (owing to the occurrence of the contact discontinuity), see figure 7. This result of the convergence was expected.

3.2. Test 2: Simple 4-shock wave

We consider now a single 4-shock wave. We assume that $M_0 \neq 0$ is given by the user. The exact solution is shown in figure 8. We propose here to examine the approximate solution of a Riemann problem, with two different

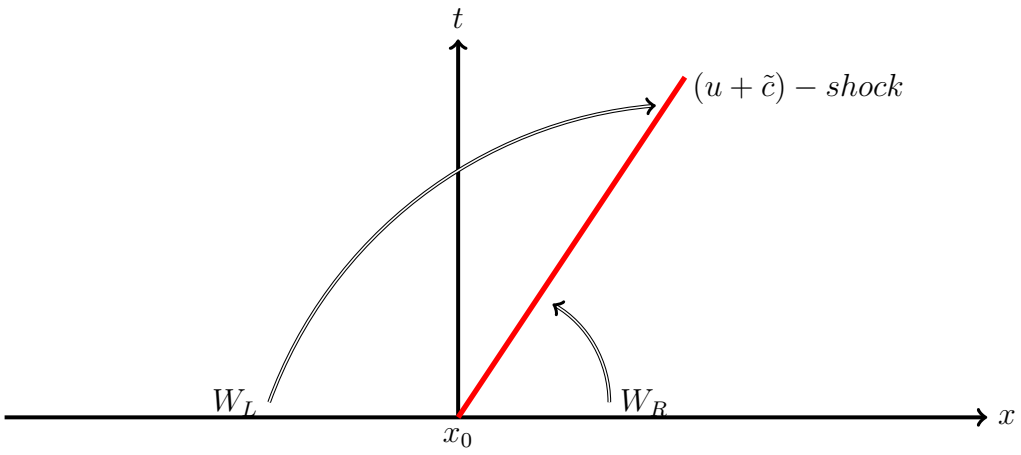

Figure 8: The exact solution of the Riemann problem for the test 2.

pressure ratios $\frac{P_L}{P_R}$, and with a strictly negative value for M_0 motivated from a physical point of view (turbulent entropy decreases through the shock). The initial condition of the Riemann problem is given by:

Case 1:

$$\sigma = 580, \text{ and } M_0 = -50000,$$

$$(\rho_L, u_L, P_L, \xi_L) = (1.936, 280.451, 261265.856, 1000)$$

$$(\rho_R, u_R, P_R, \xi_R) = (1, 650, 10^5, 913.793)$$

Case 2:

$$\sigma = 580, \text{ and } M_0 = -50000,$$

$$(\rho_L, u_L, P_L, \xi_L) = (4.487, 461.047, 268669.876, 1000)$$

$$(\rho_R, u_R, P_R, \xi_R) = (1, 650, 10^4, 913.793)$$

where W_R, σ, M_0 are given, and W_L calculated with (24).

The pressure ratio in test case 2 is close to 26.8 while the ratio in test case 1 is close to 2.6.

In the following we will perform these two test cases, with the standard scheme presented in 2.3, and with a modified scheme.

3.2.1. Standard scheme

In this part, we will illustrate the numerical results of test 2 (case 1, case 2) using the standard scheme 2.3.

Figure 9 (respectively 12) shows the behavior of the density ρ, velocity u, modified pressure P^* and turbulent entropy ξ for case 1 (respectively case 2) at a given time $T_f = 3 \times 10^{-3}$, on different meshes with 100 cells, 1000 cells and 10000 cells. Figure 10 (respectively 13) shows the convergence curve for the case 1 (respectively case 2), for the set of variables $\{\rho$, u, P, P^*,$\xi\}$. The behavior of the shock detector is shown in figure 11 (respectively 14) for case 1 (respectively case 2) on a mesh with 200000 cells.

The profiles of density ρ, velocity u, modified pressure P^*, in case 1 (rescp case 2), represented in figure 9 (respc figure 12), show a good behavior of the variable (ρ, u, P^*) through the 4-shock wave. The profiles of these 3 variables are disturbed and slightly oscillating on a coarse mesh, but by increasing the number of mesh cells, these oscillations tend to disappear. The profiles of (ρ, u, P^*) on a fine mesh take the form of the exact solution (figure 8) with x_0 = 0.674 and $T_f = 3 \times 10^{-3}$.

On the other hand, with regard to the profile of the turbulent entropy ξ, the latter converges towards the profile of the exact solution in case 2 and it does not converge in case 1.

The convergence curve ensures the above results (see figure 10 for case 1, and figure 13 for case 2). Figures 11, 14, show that the behavior of the shock detector in case 2 is better than that of case 1.

Remark 6 The parameter $coef_{i+\frac{1}{2}}$ taken in the standard scheme is a choice and not mandatory. We illustrate test 3.2 with another parameter:

$$coef_{i+\frac{1}{2}}^{n} = |P_{i+1}^{*n} - P_{i}^{*n}|. \tag{43}$$

The reader is referred to **Appendix** C for more details. ■

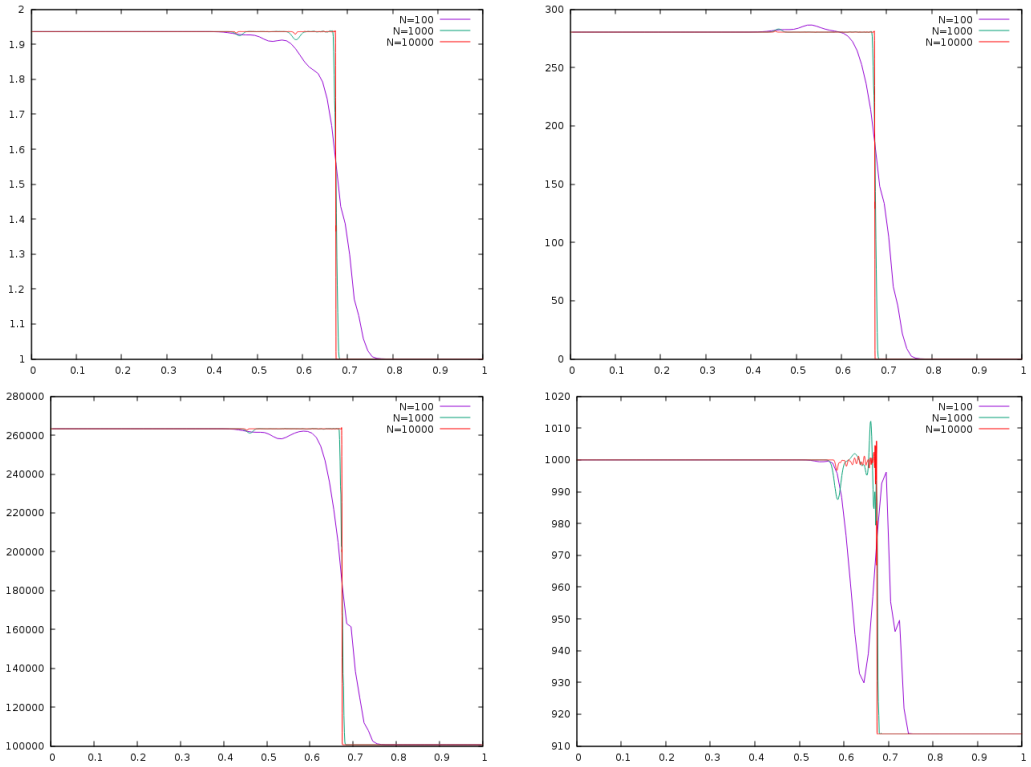

Figure 9: Simple 4-shock wave test case 1, with **standard** scheme. Density (top left), velocity (top right), P^* (bottom left) and ξ (bottom right). Profile of the approximate solution for different meshes =100, 1000, 10000 cells at $t = 3 \times 10^{-3}$ s, $CFL = 0.5$.

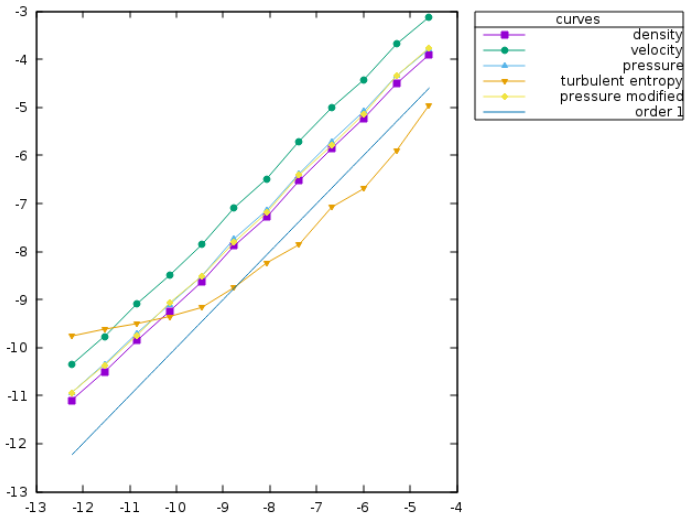

Figure 10: Simple 4-shock wave test case 1, with **standard** scheme. Convergence curves: logarithm of the relative L1-error versus the logarithm of the mesh size with uniform meshes containing from 200 to 200000 cells. The error is plotted for variables, ρ, u, P, P^* and ξ.

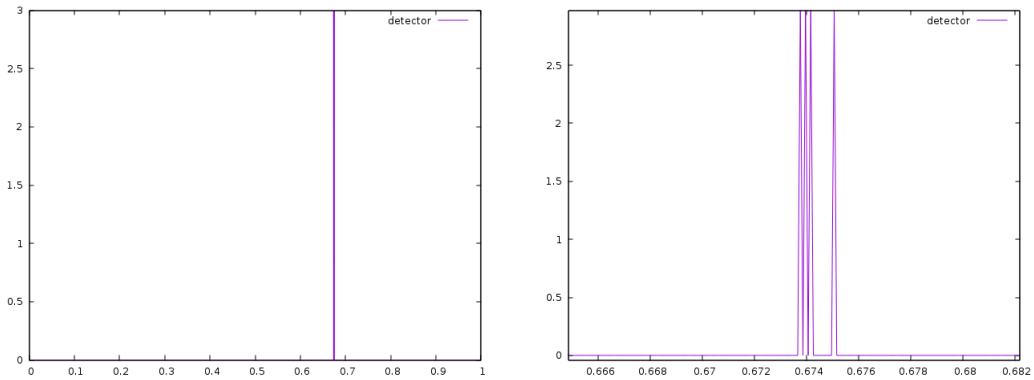

Figure 11: Simple 4-shock wave test case 1, with **standard** scheme. Shock detector behavior on all interfaces (left), behavior of the shock detector around the detected shock (right): it indicates 0 if it does not detect a shock, and 3 if it detects

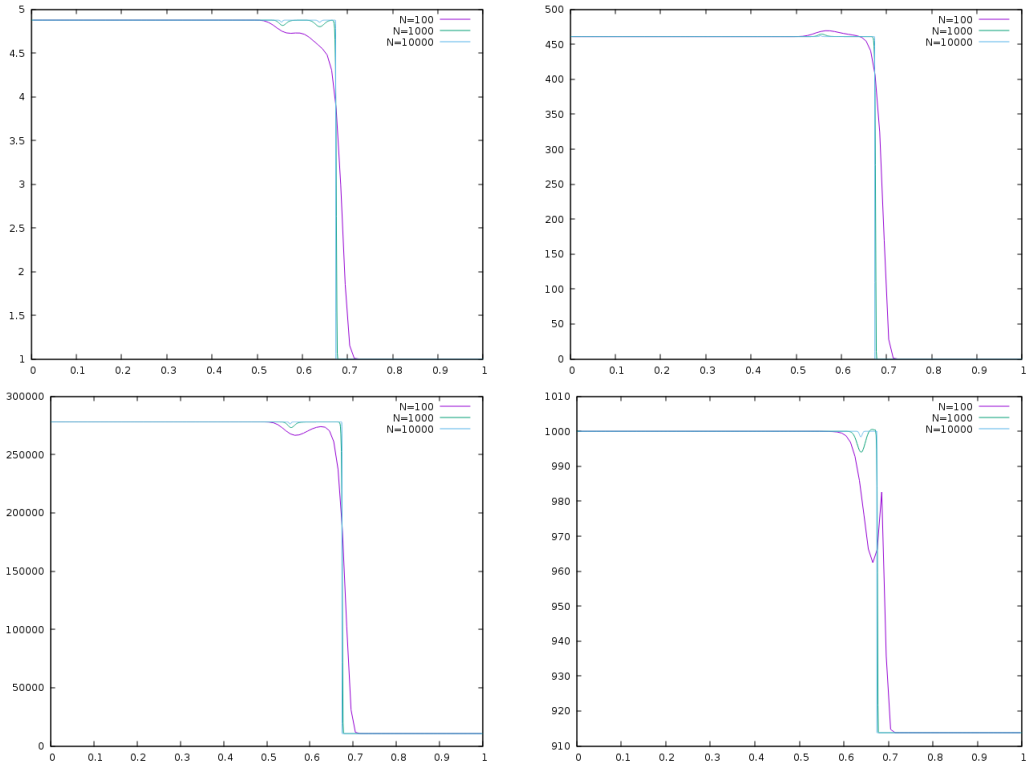

Figure 12: Simple 4-shock wave test case 2, with **standard** scheme. Density (top left), velocity (top right), P^* (bottom left) and ξ (bottom right). Profile of the approximate solution for different meshes =100, 1000, 10000 cells at $t = 3 \times 10^{-3}$ s, $CFL = 0.5$.

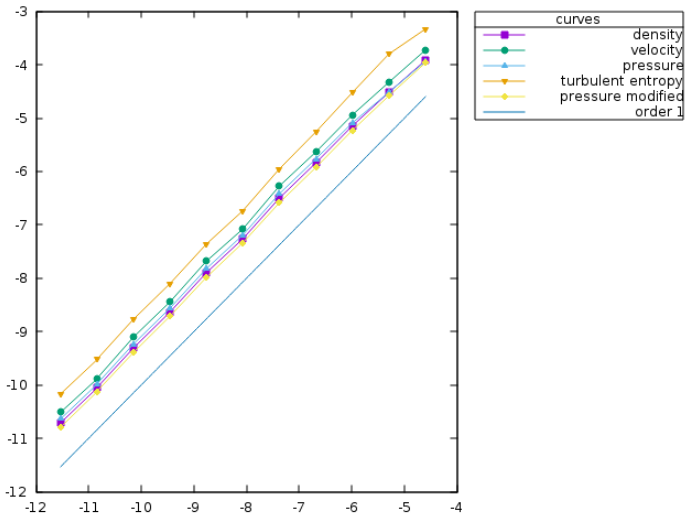

Figure 13: Simple 4-shock wave test case 2, with **standard** scheme. Convergence curves: logarithm of the relative L1-error versus the logarithm of the mesh size with uniform meshes containing from 200 to 200000 cells. The error is plotted for variables, ρ, u, P, P^* and ξ.

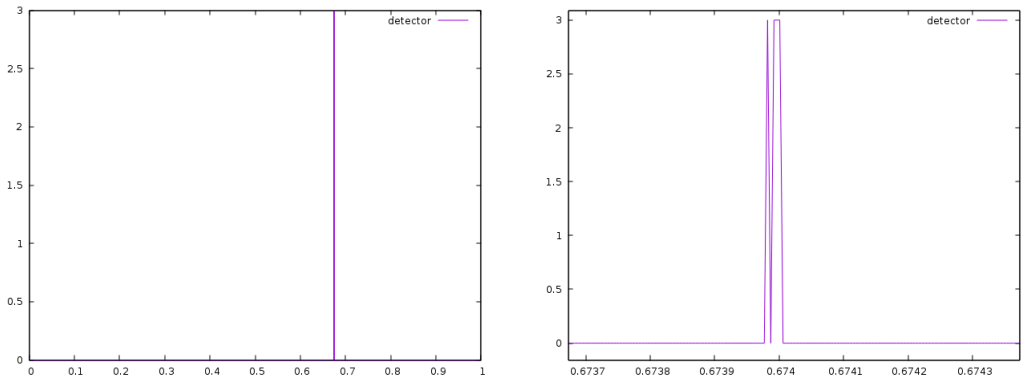

Figure 14: Simple 4-shock wave test case 2, with **standard** scheme.Shock detector behavior on all interfaces (left), behavior of the shock detector around the detected shock (right): it indicates 0 if it does not detect a shock, and 3 if it detects

3.2.2. Modified scheme

In this part, we assume that the shock is unique. We choose a single shock interface, looking for the greatest value of the jump of u:

$\max_{i=1}^{N}|u_{i+1}-u_i| = |u_{i_0+1}-u_{i_0}| \Longrightarrow$ A single shock is assumed to be located at interface $i_0+\dfrac{1}{2}$.

Consequently, we modify the numerical scheme presented in 2.3, by eliminating the 2 loops (41,42), and replace it by the following one:

$$\begin{cases} M_{i_0}^n = \frac{1}{2}M_0, \\ \\ M_{i_0+1}^n = \frac{1}{2}M_0. \end{cases}$$

In the following, we will simulate test 2 case 1 with the modified scheme. The behavior of the density ρ, velocity u, modified pressure P^* and turbulent entropy ξ, are shown in figure 15. The results provided by the two methods are almost similar for the three profiles (ρ, u, P^*). The remarkable difference between the two methods lies in the profile of the turbulent entropy, where we notice that the oscillations around the (u+$\tilde{c}$)-shock disappear on the fine meshes, whereas this is not the case with the standard scheme. The error varies as $\approx h^1$ for all variables (ρ, u, P^*, ξ), hence the convergence of all the variables with the modified scheme holds.

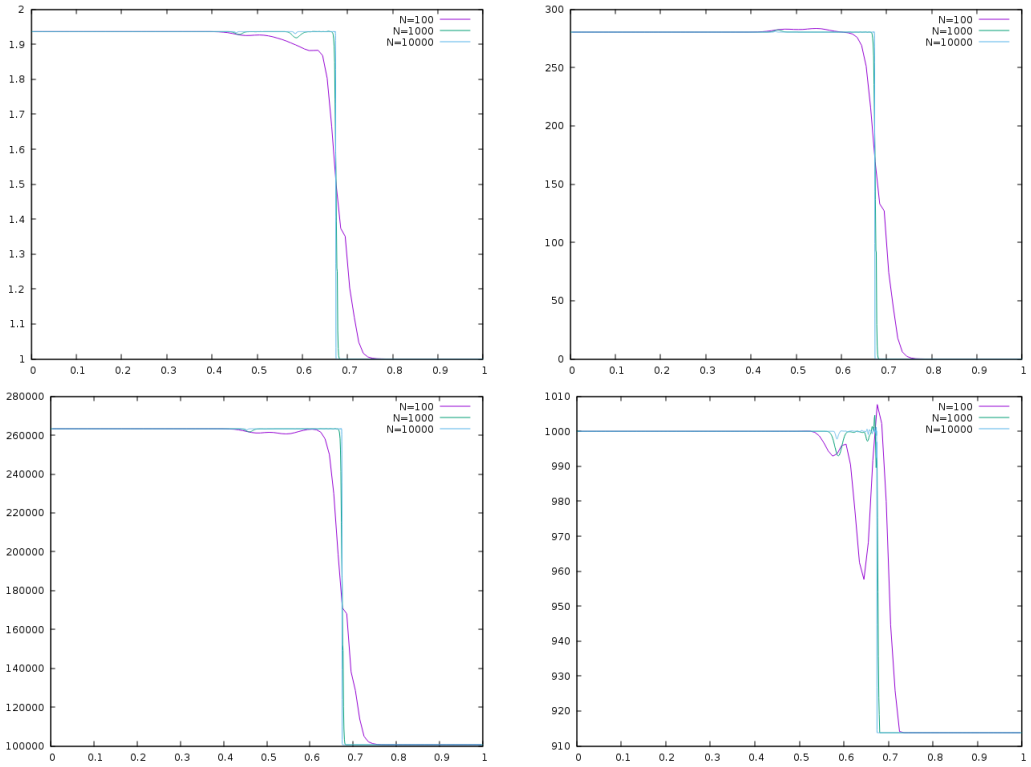

Figure 15: Simple 4-shock wave test case 1, with **modified** scheme. Density (top left), velocity (top right), P^* (bottom left) and ξ (bottom right). Profile of the approximate solution for different meshes =100 cells, 1000 cells, 10000 cells at $t = 3{\times}10^{-3}$ s, $CFL = 0.5$.

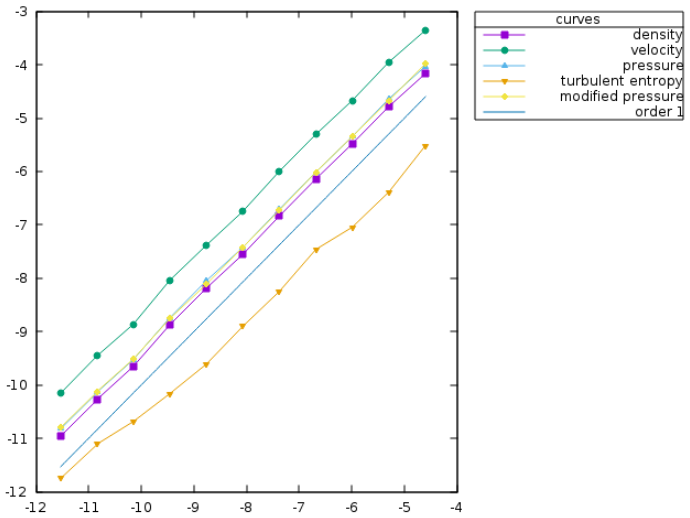

Figure 16: Simple 4-shock wave test case 1, with modified scheme. Convergence curves: logarithm of the relative L1-error versus the logarithm of the mesh size with uniform meshes containing from 200 to 200000 cells. The error is plotted for variables, ρ, u, P, P^* and ξ.

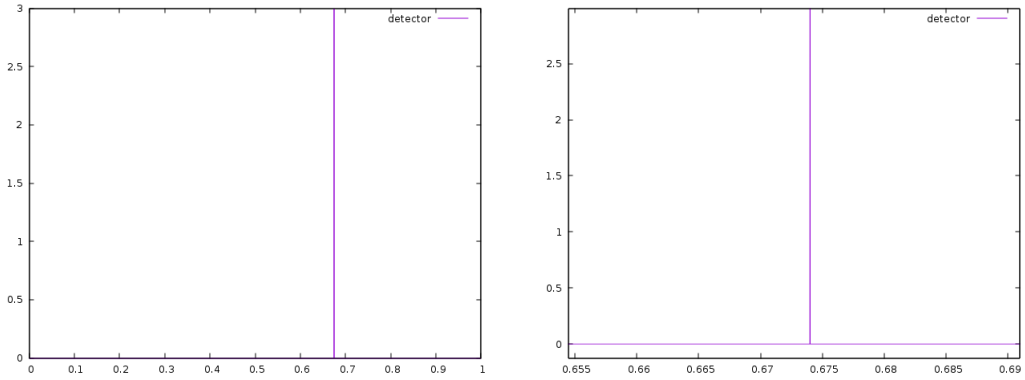

Figure 17: Simple 4-shock wave test case 1, with **modified** scheme. Shock detector behavior on all interfaces (left), behavior of the shock detector around the detected shock (right): it indicates 0 if it does not detect a shock, and 3 if it detects

4. Conclusion

This chapter was devoted to the analysis and numerical approximation of the turbulent compressible model introduced in [11]. The latter model enables to take the jump of turbulent entropy across shock waves into account, and meanwhile provides some methodology in order to calculate the entropy jump. The analysis of the model comfirms it is meaningful.
A numerical technique has been proposed in order to obtain approximate solutions when a shock wave occurs in the fluid flow. This method requires a shock detector, which has been grounded on Lax conditions and the entropy inequality. Numerical results show that the present approach must be improved in order to get consistant and stable approximations in an industrial framework.

Acknowledgements The last author receives financial support by ANRT through an EDF/CIFRE grant number 2019/1580. Computational facilities were provided by EDF.

A. Main properties of model 3 with $M(x,t) = 0$

In this section, we detail the structure of system (3) (eigenvalues, eigenvectors, Riemann invariants) in a general framework with respect to the EOS.

A.1. Hyperbolicity

System (3) is written in the form:

$$\partial_t W + A(W)\partial_x W = 0, \tag{44}$$

where the primitive variable W reads:

$$W = (\rho, u, P^*, \xi)^t.$$

The jacobian matrix A(W) is:

$$A(W) = \begin{pmatrix} u & \rho & 0 & 0 \\ 0 & u & \tau & 0 \\ 0 & \rho\tilde{c}^2 & u & 0 \\ 0 & 0 & 0 & u \end{pmatrix},$$

where $\tau = 1/\rho$ denotes the specific volume and $\tilde{c}^2 = c^2(P,\rho) + \frac{10}{9}\xi\rho^{2/3}$.

System (44) is hyperbolic, it admits four real eigenvalues:

$$\lambda_1(W) = u - \tilde{c}, \quad \lambda_{2,3}(W) = u, \quad \lambda_4(W) = u + \tilde{c}, \tag{45}$$

and the associated eigenvectors r_k(W) span the whole space $\mathbb{R}^4$ provided that $\tilde{c} \neq 0$:

$$r_1(W) = \left(\rho, -\tilde{c}, \rho\tilde{c}^2, 0\right)^t, \quad r_2(W) = (1,0,0,0)^t,$$

$$r_3(W) = (0,0,0,1)^t\,, \quad r_4(W) = \left(\rho, \tilde{c}, \rho\tilde{c}^2, 0\right)^t.$$

Fields associated with $\lambda_1(W)$ *and* $\lambda_4(W)$ are genuinely non linear (GNL), and field associated with $\lambda_{2,3}(W)$ is linearly degenerate (LD).

A.2. Riemann invariants

The two Riemann invariants associated with the LD field ($\lambda_{2,3} = u$) are the following whatever the **EOS** is:

$$I_1^2(W) = u \quad , \quad I_2^2(W) = P^*(P,\rho,\xi).$$

The Riemann invariants associated with the two GNL waves read:

$$1-rarefaction\ wave: \ \ I_1^1(W) = s(P,\rho)\ ,\ \ I_2^1(W) = u + \int_0^\rho \frac{\tilde{c}(I_1^1(W),\rho\prime,I_3^1(W))}{\rho\prime}\,\mathrm{d}\rho\prime,$$

$$1-rarefaction\ wave: \ \ I_3^1(W) = \xi.$$

$$4-rarefaction\ wave: \ \ I_1^4(W) = s(P,\rho)\ ,\ \ I_2^4(W) = u - \int_0^\rho \frac{\tilde{c}(I_1^4(W),\rho\prime,I_3^4(W))}{\rho\prime}\,\mathrm{d}\rho\prime,$$

$$4-rarefaction\ wave: \ \ I_3^4(W) = \xi.$$

B. The intermediate states for VFRoe-ncv

The VFRoe-ncv scheme is based on the computation of the exact solution of a linearized version of the Riemann problem at the interface between two cells. It thus relies on finding the two intermediate states Z_1 and Z_2: the state Z_1 (resp. Z_2) lies between the linearized waves $\bar{\lambda}_1$ and $\bar{\lambda}_{2,3}$ (resp. $\bar{\lambda}_{2,3}$ and $\bar{\lambda}_4$). We have:

$$Z_1 = Z_L + \alpha_1 \widehat{r}_1, \tag{46}$$

$$Z_2 = Z_1 + \alpha_2 \widehat{r_2} + \alpha_3 \widehat{r_3}, \tag{47}$$

$$Z_R = Z_2 + \alpha_4 \widehat{r_4}, \tag{48}$$

where the linearized right eigenvectors are:

$$\widehat{r_1} = (1, -\widehat{\tilde{c}}\tau, \widehat{\tilde{c}}^2, 0)^t, \quad \widehat{r_2} = (1,0,0,0)^t, \quad \widehat{r_3} = (0,0,0,1)^t, \quad \widehat{r_4} = (1, \widehat{\tilde{c}}\tau, \widehat{\tilde{c}}^2, 0)^t,$$

and where the coefficients α_1 and α_4 associated with the eigenvalues $\bar{\lambda}_1$ and $\bar{\lambda}_4$ read:

$$\alpha_1 = \frac{1}{2}\frac{[P^*]_L^R}{\widehat{\tilde{c}}^2} - \frac{1}{2}\frac{[u]_L^R \widehat{\rho}}{\widehat{\tilde{c}}},$$

$$\alpha_4 = \frac{1}{2}\frac{[P^*]_L^R}{\widehat{\tilde{c}}^2} + \frac{1}{2}\frac{[u]_L^R \widehat{\rho}}{\widehat{\tilde{c}}}.$$

It should be noted that thanks to (47), we have:

$$u_1 = u_2, \quad \text{and} \quad P_1^* = P_2^*.$$

After simple calculus on equations (46) and (48), the following intermediate values can be found:

$$u_1 = u_2 = \bar{u} - \frac{1}{2\bar{\rho}\widehat{\tilde{c}}}[P^*]_L^R,$$

$$P_1^* = P_2^* = \bar{P^*} - \frac{\bar{\rho}\widehat{\tilde{c}}}{2}[u]_L^R,$$

$$\rho_1 = \rho_L + \frac{[P^*]_L^R}{2\widehat{\tilde{c}}^2} - \frac{\bar{\rho}}{2\widehat{\tilde{c}}}[u]_L^R, \quad \rho_2 = \rho_R - \frac{[P^*]_L^R}{2\widehat{\tilde{c}}^2} - \frac{\bar{\rho}}{2\widehat{\tilde{c}}}[u]_L^R,$$

$$\xi_1 = \xi_L, \quad \xi_2 = \xi_R.$$

Finally, the intermediate states are defined as follows:

$$W_k^{lnd} = (\rho_k, u_k, P_k^*, \xi_k), \ k = 1, 2. \tag{49}$$

C. Additional numerical results: a simple 3-shock wave with different coefficients

The profiles of the approximate solutions along the x-domain are given in figure 18 (respectively 21) for case 1 (respectively case 2), for several meshes with 100, 1000 and 10000 cells. Figure 19 (respectively 22) represents the error curve for case 1 (respectively case 2), and the shock detector behavior is shown in figure 20 (respectively 23) for case 1 (respectively case 1).

Finally, by comparing these results (with $coef^n_{i+\frac{1}{2}} = |P^{*n}_{i+1} - P^{*n}_i|$) with the results of part 3.2.1 (with $coef^n_{i+\frac{1}{2}} = |\rho^n_{i+1} - \rho^n_i|$), we find that the solution is roughly almost the same.

D. A tentative PDE formulation of model [11]

Model [11] provides the contents of M_0 (see section 1.2). System of equations (3) presented in section 1, can be rewritten as follows:

$$\begin{cases} \partial_t\phi + \sigma\partial_x\phi = 0 \\ \partial_t(\rho) + \partial_x(\rho u) = 0 \\ \partial_t(\rho u) + \partial_x\left(\rho u^2 + P + \dfrac{2K}{3}\right) = 0 \\ \partial_t(\rho E) + \partial_x\left(u\left(\rho E + P + \dfrac{2K}{3}\right)\right) = 0 \\ \partial_t(\rho\xi) + \partial_x(\rho u\xi) + M_0\partial_x\phi = 0 \end{cases} \tag{50}$$

by noting the mean total energy E:

$$E = e + \frac{1}{2}u^2 + \frac{K}{\rho}.$$

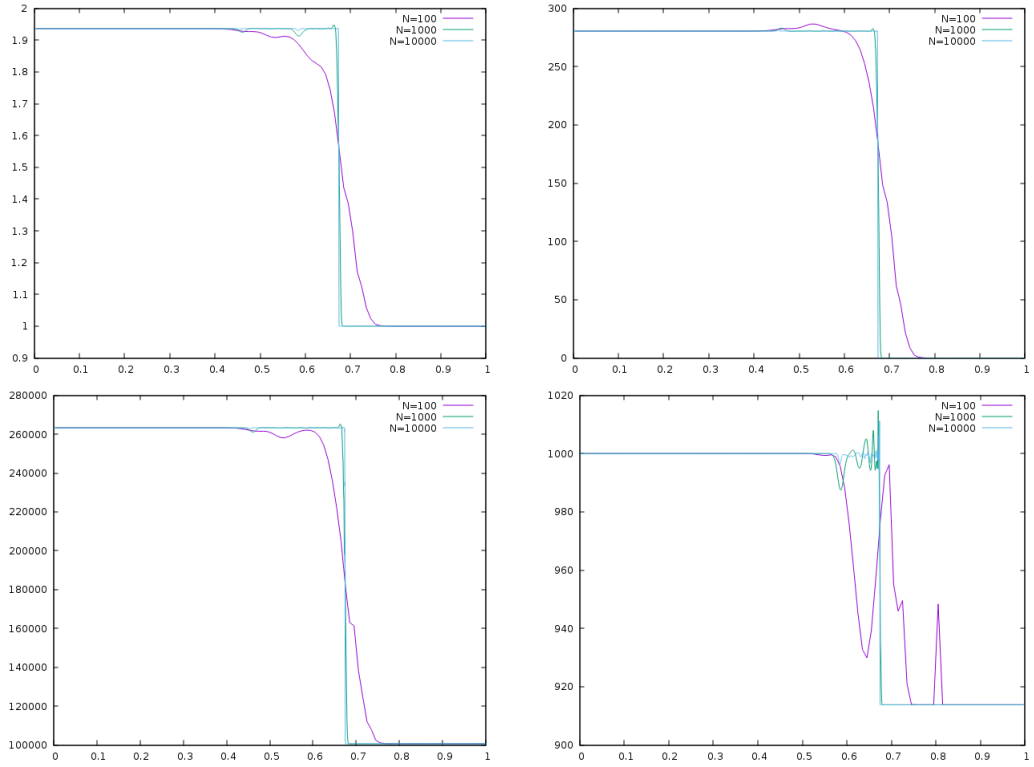

Figure 18: Simple 3-shock wave test case 1, with standard scheme and $coef_{i+1/2} = |P^*_{i+1} - P^*_i|$. Density (top left), velocity (top right), P^* (bottom left) and ξ (bottom right). Profile of the approximate solution for different meshes =100, 1000, 10000 cells at $t = 3 \times 10^{-3}$ s, $CFL = 0.5$.

We define the modified pressure P^*:

$$P^* = P + \frac{2}{3}K,$$

where $K = \xi\rho^{5/3} \Longleftrightarrow \xi = K\rho^{-5/3}$.

The variable ϕ denotes a colour function (see [16, 15, 12, 1] such that:

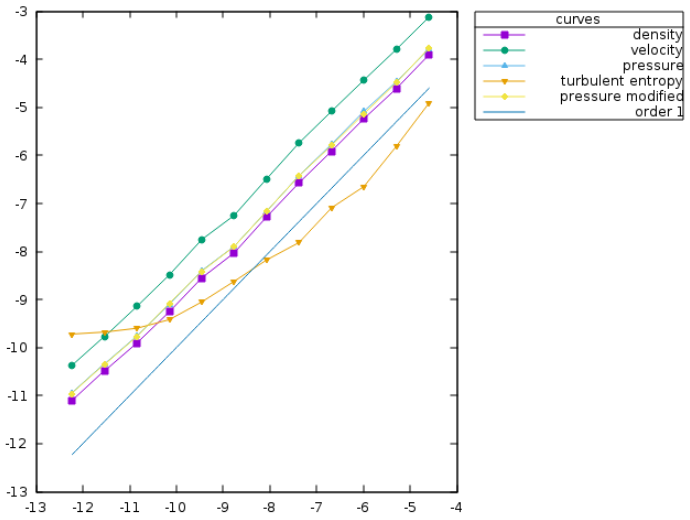

Figure 19: Simple 3-shock wave test case 1, with standard scheme and $coef_{i+1/2} = |P^*_{i+1} - P^*_i|$. Convergence curves: logarithm of the relative L1-error versus the logarithm of the mesh size with uniform meshes containing from 200 to 200000 cells. The error is plotted for variables, ρ, u, P, P^* and ξ.

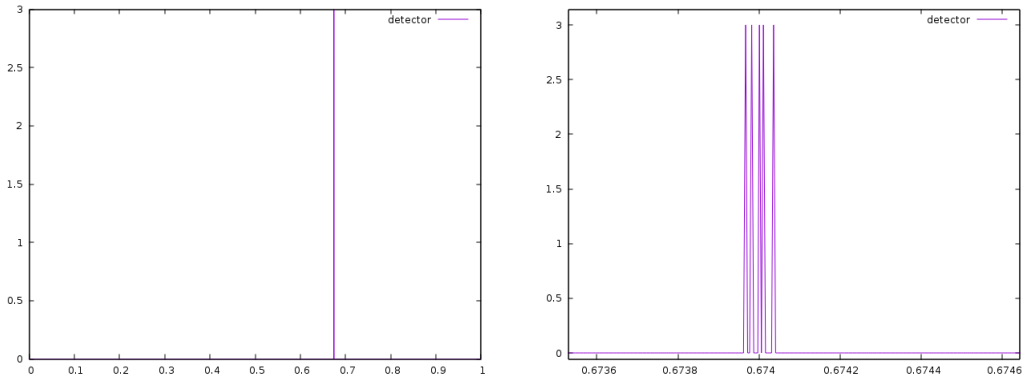

Figure 20: Simple 3-shock wave test case 1, with standard scheme and $coef_{i+1/2} = |P^*_{i+1} - P^*_i|$. Shock detector behavior on all interfaces (left), behavior of the shock detector around the detected shock (right): it indicates 0 if it does not detect a shock, and 3 if it detects

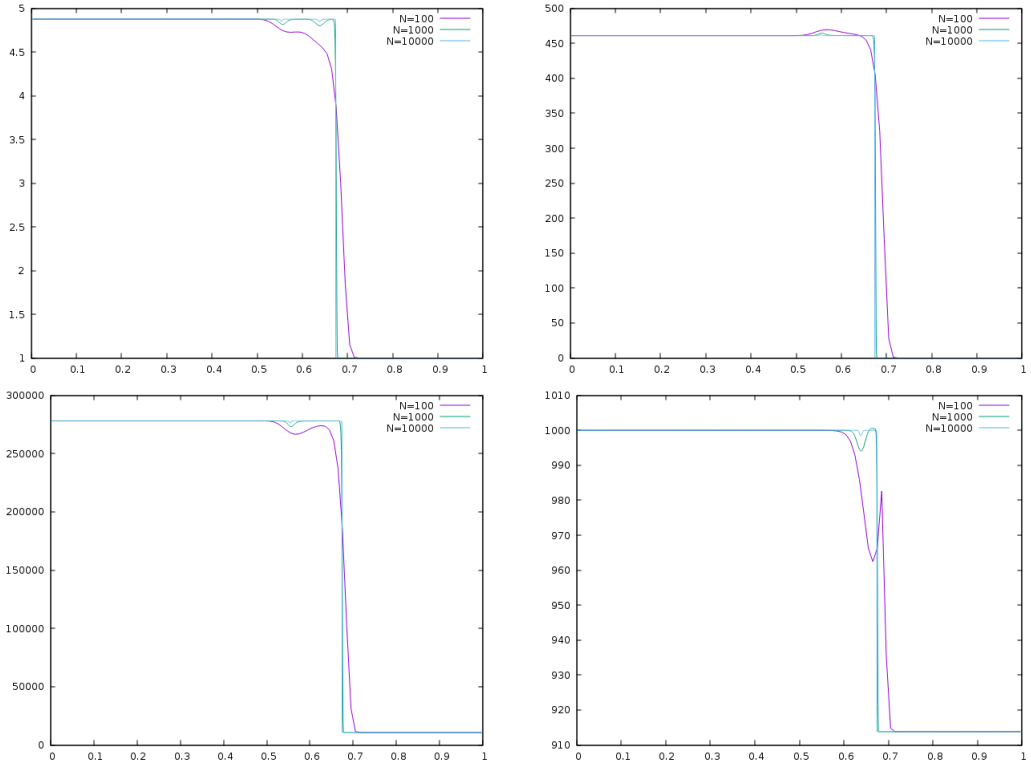

Figure 21: Simple 3-shock wave test case 2, with standard scheme and $coef_{i+1/2} = |P^*_{i+1} - P^*_i|$. Density (top left), velocity (top right), P^* (bottom left) and ξ (bottom right). Profile of the approximate solution for different meshes =100, 1000, 10000 cells at $t = 3 \times 10^{-3}$ s, $CFL = 0.5$.

$$\phi(x,0) = \begin{cases} 0 & \text{if} \quad x < 0 \\ 1 & \text{if} \quad x > 0 \end{cases}$$

and σ is the shock speed. M_0 is given non zero.

System (50) is rewritten as follows:

$$\partial_t Y + C(Y)\partial_x Y = 0, \tag{51}$$

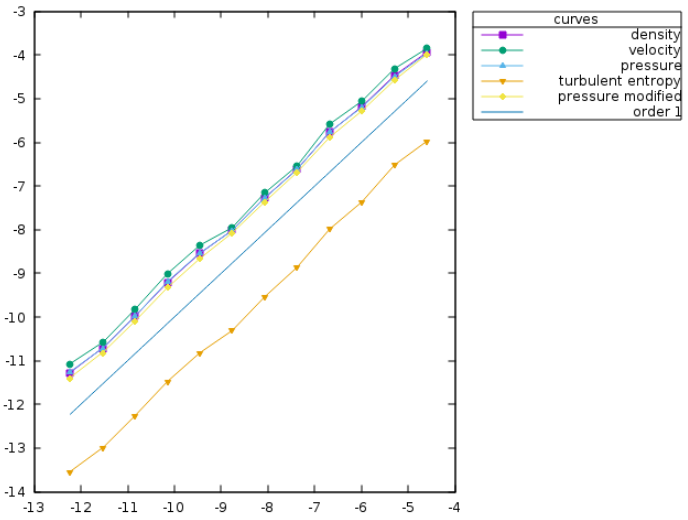

Figure 22: Simple 3-shock wave test case 2, with **standard** scheme and $coef_{i+1/2} = |P^*_{i+1} - P^*_i|$. Convergence curves: logarithm of the relative L1-error versus the logarithm of the mesh size with uniform meshes containing from 200 to 200000 cells. The error is plotted for variables, ρ, u, P, P^* and ξ.

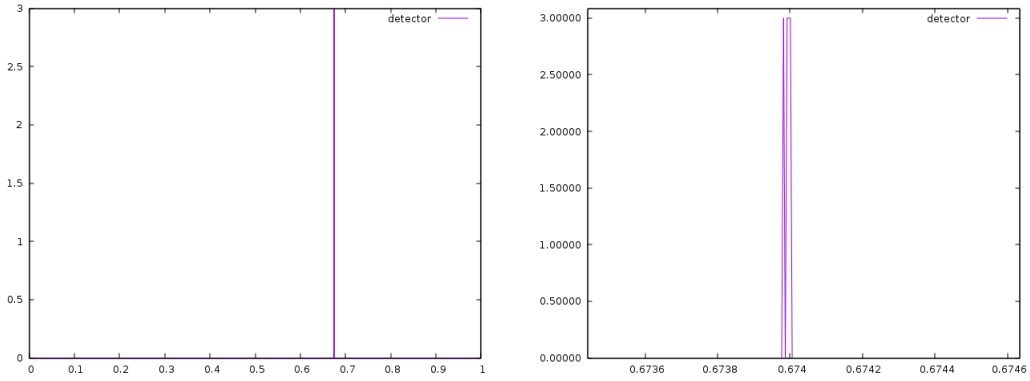

Figure 23: Simple 3-shock wave test case 2, with **standard** scheme and $coef_{i+1/2} = |P^*_{i+1} - P^*_i|$. Shock detector behavior on all interfaces (left), behavior of the shock detector around the detected shock (right): it indicates 0 if it does not detect a shock, and 3 if it detects

with Y the primitive variable:

$$Y = (\phi, \rho, u, P^*, \xi),$$

$C(Y)$ is the jacobian matrix:

$$C(Y) = \begin{pmatrix} \sigma & 0 & 0 & 0 & 0 \\ 0 & u & \rho & 0 & 0 \\ 0 & 0 & u & \tau & 0 \\ A & 0 & \rho\tilde{c}^2 & u & 0 \\ B & 0 & 0 & 0 & u \end{pmatrix},$$

with:

$$\begin{cases} A = M_0 \rho^{-1/3} \left(\frac{2}{3}\rho - (\frac{\partial e}{\partial P}|_\rho)^{-1} \right), \\ B = \frac{M_0}{\rho}. \end{cases} \tag{52}$$

We assume that: $M_0 \neq 0$, and $\gamma \neq \frac{5}{3}$ (in case of a perfect gas EOS) which implies that:

$$\mathbf{A \neq 0 \text{ and } B \neq 0}.$$

System (51) admits five real eigenvalues:

$$\lambda_0(Y) = \sigma, \quad \lambda_1(Y) = u - \tilde{c}, \quad \lambda_{2,3}(Y) = u, \quad \lambda_4(Y) = u + \tilde{c}. \tag{53}$$

The associated eigenvectors $r_k(Y)$ are:

$$r_0(Y) = \left(\Delta(u-\sigma), -A, (u-\sigma)\frac{A}{\rho}, -A(u-\sigma)^2, -B\Delta \right)^t,$$

$$r_1(Y) = \left(0, \rho, -\tilde{c}, \rho\tilde{c}^2, 0\right)^t, \quad r_2(Y) = (0,1,0,0,0)^t,$$

$$r_3(Y) = (0,0,0,0,1)^t, \quad r_4(Y) = \left(0, \rho, \tilde{c}, \rho\tilde{c}^2, 0\right)^t,$$

with $\Delta = (u-\sigma)^2 - \tilde{c}^2$.

In the sequel, we assume that:

$$\sigma \neq u.$$

We must distinguish two cases which depend on the value of Δ:
(i) $\Delta \neq 0$: system (50) is hyperbolic (eigenvectors span $\mathbb{R}^5$);
(ii) $\Delta = 0$: the associated eigenvector $r_0(Y) \in Vect\{r_1, r_2, r_4\} \Longrightarrow$ system (50) is degenerate.

The second case (ii) above corresponds to system (3) **in section 1.1.**

E. Positivity of the total pressure of the mixture P^*

In this section, we are interested in studying the condition of the positivity of the total pressure of the mixture P^*. Let us first recall the system of Rankine-Hugoniot relations associated with model (3). We assume that the variable $(\rho, u, P, \xi)_R$ on the right side of the shock 'R', the shock speed σ and M_0 are given. The system of jump conditions is written as follows:

$$\begin{cases} [\rho(u-\sigma)]_2^R = 0 \\ m^2[\tau]_2^R + [P^*]_2^R = 0 \\ [e + K\tau]_2^R + \bar{P}^*_{R,2}[\tau]_2^R = 0 \\ m[\xi]_2^R + M_0 = 0 \end{cases} \tag{54}$$

with $P^* = P + \frac{2}{3}K$, $\tau = \frac{1}{\rho}$, $K = \xi\rho^{5/3}$ and $m = \rho_R(u_R - \sigma)$. The variable $(\rho, u, P, \xi)_2$ on the left side of the shock noted '2' is the main unknown.

In the sequel, we will consider the following turbulent perfect gas EOS:

$$P = (\gamma - 1)\rho e.$$

The third equation of system (54) can be written in the following form:

$$\begin{cases} P_2^* = P_R^* g(z) \\ g(z) = \dfrac{h(z)}{(\beta - z)} \\ h(z) = \beta z - 1 + 2\dfrac{(\gamma - 5/3)}{(\gamma - 1)}(\dfrac{K_R}{P_R^*})(z - \dfrac{K_2}{K_R}) \\ z = \dfrac{\rho_2}{\rho_R} \end{cases} \tag{55}$$

To study the positivity of P^*, we will examine the variation of the function $h(z)$ in the interval $[1, \beta[$. The derivative of the function h(z) is:

$$h'(z) = \beta + 2\frac{(\gamma - 5/3)}{(\gamma - 1)}\frac{K_R}{P_R^*}.$$

We distinguish 2 cases which depend on the value of γ:

- for γ>5/3: h'(z) is positive in the interval [1,β[$\Longrightarrow$ h(z) is increasing over [1,β[; then for h(z) to be positive ($P_2^* > 0$), it suffices that h(1)>0, which imposes a condition on the jump of $[K]_2^R$ such that:

$$P_R^* + (\gamma - 5/3)[K]_2^R > 0 \iff h(1) > 0 \tag{56}$$

- for $\gamma < 5/3$: we distinguish 2 sub-cases:

  1. if $(\gamma + 1) + 2(\gamma - 5/3)\frac{K_R}{P_R^*} > 0$: h'(z) is positive in the interval [1,β[$\Longrightarrow$ h(z) is increasing in [1,β[; condition (56) appears to keep the positivity of $P*$.

2. if $(\gamma+1)+2(\gamma-5/3)\frac{K_R}{P_R^*} < 0$: $h'(z)<0$ in $[1,\beta[\Longrightarrow h(z)$ is decreasing in $[1,\beta[$; then for $h(z)>0$ ($P_2^* > 0$), it suffices that $h(\beta)>0$, which imposes a condition on the jump of $[K]_2^R$ such that:

$$\gamma P_R + \frac{5}{3}(\gamma-1)K_R + \frac{(\gamma-1)(\gamma-5/3)}{2}[K]_2^R > 0.$$

F. Study of the ratio $\frac{P_2^*}{P_R^*}$ in (u+$\tilde{c}$)-shock

First of all, let us define P_k:

$$P_k = \frac{2}{3}K,$$

so that the pressure P^* reads:

$$P = P + P_k.$$

The modified pressure P^* is then composed of a 'laminar' thermodynamical pressure P and a 'turbulent' contribution P_k. In the following, the ratio $\frac{P_2^*}{P_R^*}$ is studied for the model considering a turbulent perfect gas EOS:

$$P = (\gamma-1)\rho e.$$

We assume that the right state $(\rho, u, P, \xi)_R$ and σ are known, and that $P_{k,R} > 0$ and $P_R > 0$. The jump relations associated with (u+$\tilde{c}$)-shock are:

$$\begin{cases} [\rho(u-\sigma)]_2^R = 0 \\ m^2[\tau]_2^R + [P^*]_2^R = 0 \\ [e + K\tau]_2^R + \bar{P}_{R,2}^*[\tau]_2^R = 0 \\ m[\xi]_2^R + M_0 = 0 \\ \frac{4}{3}\xi_2\tau_R^{-2/3}\alpha = P_R^* + P_2^*\beta + m^2\tau_R - m^2\tau_2\beta \end{cases} \tag{57}$$

with $m = \rho_R(u_R - \sigma)$, $\alpha = \frac{(\gamma-5/3)}{(\gamma-1)}$, $\beta = \frac{(\gamma+1)}{(\gamma-1)}$, σ is the speed of the shock and $P^* = P + \frac{2}{3}\xi\rho^{5/3}$ is the total pressure.

We set:

$$z_2 = \frac{\rho_2}{\rho_R}.$$

Across a (u+$\tilde{c}$)-shock wave we have necessarily $z_2 > 1$ and $z_2 < \frac{(\gamma+1)}{\gamma}$ (see section 1.2). Using the third and fifth equations of (57), we get the following formula for the pressure P_2^* with respect to z_2 and to the right state:

$$P_2^* = P_R^* h_2(z_2; \xi_R, P_R^*, \rho_R), \tag{58}$$

with:

$$h_2(z_2; \xi_R, P_R^*, \rho_R) = \frac{2\beta z_2^2 - 5z_2 + 4z_2^2 \frac{K_R}{P_R^*}\alpha - 3m^2 \frac{\tau_R}{P_R^*}(z_2 - \beta)}{5z_2(\beta - \frac{2}{5}z_2)} \tag{59}$$

We note that the jump relations (57) can only be defined if $h_2(z_2; \xi_R, P_R^*, \rho_R) > 1$ (thanks to the second equation of relations of jump). For this, we examine below the conditions to keep $(h_2(z_2; \xi_R, P_R^*, \rho_R) - 1) > 0$ with respect to $z_2 \in [1, \frac{(\gamma+1)}{\gamma}[$.

First of all:

$$h_2(z_2; \xi_R, P_R^*, \rho_R) - 1 = \frac{g_2(z_2; \xi_R, P_R^*, \rho_R)}{5z_2(\beta - \frac{2}{5}z_2)},$$

with:

$$g_2(z_2; \xi_R, P_R^*, \rho_R) = 2z_2^2(\beta + 2\frac{K_R}{P_R^*}\alpha + 1) + z_2(-5 - 5\beta - 3m^2\frac{\tau_R}{P_R^*}) + 3m^2\frac{\tau_R}{P_R^*}\beta. \tag{60}$$

Since $5z_2(\beta - \frac{2}{5}z_2) > 0$ (because$z_2 < \frac{(\gamma+1)}{\gamma}$) is positive. The positivity study of g_2 is equivalent to $(h_2(z_2; \xi_R, P_R^*, \rho_R) - 1) > 0$.

The first and second order derivatives of g_2 are:

$$g\prime_2(z_2) = 4z_2(\beta + 2\frac{K_R}{P_R^*}\alpha + 1) - 5 - 5\beta - 3m^2\frac{\tau_R}{P_R^*}, \tag{61}$$

$$g\prime\prime_2(z_2) = 4(\beta + 2\frac{K_R}{P_R^*}\alpha + 1). \tag{62}$$

We distinguish 2 cases for $g\prime\prime(z_2)$ depending on the sign of α (γ):

1. if $\alpha > 0$ ($\gamma > 5/3$): we have $g\prime\prime_2(z_2)$ positive for $z_2 \in [1, \frac{(\gamma+1)}{\gamma}[$
2. if $\alpha < 0$ ($\gamma < 5/3$): We distinguish 2 cases depending on ratio value $\frac{P_{K,R}}{P_R^*}$:
   (a) if $\frac{P_{K,R}}{P_R^*} < \frac{2\gamma}{3(5/3-\gamma)}$: we have $g\prime\prime_2(z_2)$ positive for $z_2 \in [1, \frac{(\gamma+1)}{\gamma}[$
   (b) if $\frac{P_{K,R}}{P_R^*} > \frac{2\gamma}{3(5/3-\gamma)}$: we have $g\prime\prime_2(z_2)$ negative for $z_2 \in [1, \frac{(\gamma+1)}{\gamma}[$

The case $\gamma > 5/3$ is not relevant (see section 1.2), we are interested in the case $\gamma < 5/3$ in the following.

For $\gamma < 5/3$: we have distinguished 2 sub-cases, which depend on the value of the ratio $\frac{P_{K,R}}{P_R^*}$. The limiting ratio is bounded by $\delta = \frac{2\gamma}{3(5/3-\gamma)} > 1$ ($\gamma < \frac{5}{3}$), then case(b) $\frac{P_{K,R}}{P_R^*} > 1$ then case (b) is impossible. For that purpose, we will consider that case 2(a) in the study of the positivity of $g_2(z_2)$.

Case 2(a): $\gamma < \frac{5}{3}$ and $\frac{K_R}{P_R^*} < \frac{\gamma}{(5/3-\gamma)}$: we have $g\prime\prime_2(z_2)$ positive $\forall\ z_2 \in [1, \frac{(\gamma+1)}{\gamma}[$, which implies that $g\prime(z_2)$ is increasing $\forall\ z_2 \in [1, \frac{(\gamma+1)}{\gamma}[$.
Sign of g$\prime_2$: thanks to condition 2(a), we find that $g\prime_2(\frac{(\gamma+1)}{\gamma}) < 0$, but since $g\prime_2$ is an increasing function, then $g\prime_2(z_2)$ is negative $\forall\ z_2 \in [1, \frac{(\gamma+1)}{\gamma}[$. This implies that the function $g_2(z_2)$ is decreasing $\forall\ z_2 \in [1, \frac{(\gamma+1)}{\gamma}[$.

Finally for $\gamma < \frac{5}{3}$ and $\frac{K_R}{P_R^*} < \frac{\gamma}{(5/3-\gamma)}$: $g_2(z_2)$ is decreasing in $[1, \frac{(\gamma+1)}{\gamma}[$; then for getting $g_2(z_2) > 0$ ($P_2^* > P_R^*$), it suffices that $g_2(\frac{(\gamma+1)}{\gamma}) > 0$, which imposes the following condition:

$$2(\frac{(\gamma+1)}{\gamma})^2 \left(\beta + 1 + 2\frac{K_R}{P_R^*}\alpha\right) + \frac{(\gamma+1)}{\gamma}\left(-5 - 5\beta - 3m^2\frac{\tau_R}{P_R^*}\right) + 3m^2\frac{\tau_R}{P_R^*}\beta > 0. \tag{63}$$

References

[1] Annalisa Ambroso, Christophe Chalons, Frédéric Coquel, and Thomas Galié. Relaxation and numerical approximation of a two-fluid two-pressure diphasic model. *ESAIM: Mathematical Modelling and Numerical Analysis*, 43(6):1063–1097, 2009.

[2] Christophe Berthon. *Contribution à l'analyse numérique des équations de Navier-Stokes compressibles à deux entropies spécifiques. Applications à la turbulence compressible.* PhD thesis, Paris 6, 1999.

[3] Christophe Berthon and Frédéric Coquel. Nonlinear projection methods for multi-entropies navier-stokes systems, https://doi.org/10.1142/9789812810816_0014. *Innovative Methods For Numerical Solution Of Partial Differential Equations*, pages 278–304, 2002.

[4] Thierry Buffard, Thierry Gallouët, and Jean-Marc Hérard. A sequel to a rough Godunov scheme: application to real gases. *Computers & Fluids*, 29(7):813–847, 2000.

[5] Robert Eymard, Thierry Gallouët, and Raphaèle Herbin. *Finite volume methods.* Elsevier, 2000.

[6] Alexandre Favre. Equations statistiques des gaz turbulents. *Compte-Rendus de l'Académie des Sciences Paris*, 246(18):2576–2579, 1958.

[7] Alexandre Favre. Equations des gaz turbulents compressibles. 1, formes générales. 2, méthode des vitesses moyennes; méthode des vitesses

macroscopiques pondérées par la masse volumique. *Journal de Mécanique*, 4(3), 1965.

[8] Alexandre Favre, Leslie S.G. Kosvaznay, Raymond Dumas, Jean Gaviglio, and Michel Coantic. *La turbulence en mécanique des fluides: bases théoriques et expérimentales, méthodes statistiques*. Gauthier-Villars, 1976.

[9] Thomas B Gatski and Jean-Paul Bonnet. *Compressibility, turbulence and high speed flow*. Academic Press, 2013.

[10] Sergey Gavrilyuk, Jean-Marc Hérard, Olivier Hurisse, and Ali Toufaili. Theoretical and numerical analysis of a simple model derived from compressible turbulence. *Journal of Mathematical Fluid Mechanics*, 24(2):1–34, 2022.

[11] Sergey Gavrilyuk and Richard Saurel. Estimation of the turbulent energy production across a shock wave. *Journal of Fluid Mechanics*, 549:131, 2006.

[12] Paola Goatin and Philippe G LeFloch. The riemann problem for a class of resonant hyperbolic systems of balance laws. In *Annales de l'Institut Henri Poincaré C, Analyse non linéaire*, volume 21, pages 881–902. Elsevier, 2004.

[13] Edwige Godlewski and Pierre-Arnaud Raviart. *Numerical approximation of hyperbolic sytems of conservation laws*. Springer Berlin, 1996.

[14] Sergueï Konstantinovitch Godunov. A difference method for numerical

calculation of discontinuous equations of hydrodynamics. *Math sbornik (in Russian)*, 47(89)(3):271–306, 1959.

[15] Laurent Gosse. A well-balanced scheme using non-conservative products designed for hyperbolic systems of conservation laws with source terms. *Mathematical Models and Methods in Applied Sciences*, 11(02):339–365, 2001.

[16] Joshua M Greenberg and Alain-Yves LeRoux. A well-balanced scheme for the numerical processing of source terms in hyperbolic equations. *SIAM Journal on Numerical Analysis*, 33(1):1–16, 1996.

[17] Jean-Marc Hérard. Technical report, A simple turbulent model for compressible flows, https://hal.archives-ouvertes.fr/hal-02007044, 2014.

[18] Jean-Marc Hérard and Hippolyte Lochon. A simple turbulent two-fluid model. *Comptes Rendus Mécanique*, 344(11-12):776–783, 2016.

[19] Masashi Kanamori and Kojiro Suzuki. Shock wave detection in two-dimensional flow based on the theory of characteristics from cfd data. *Journal of Computational Physics*, 230(8):3085–3092, 2011.

[20] Stephen B Pope. *Turbulent flows*. Cambridge university press, 2000.

[21] Joel Smoller. *Shock waves and reaction—diffusion equations*. Springer Science & Business Media, 1983.

[22] Philippe Spalart and Steven Allmaras. A one-equation turbulence model for aerodynamic flows, https://arc.aiaa.org/doi/10.2514/6.1992-439. *La Recherche Aérospatiale*, pages 5–21, 1994.

[23] Henk Tennekes and John Leask Lumley. A first course in turbulence. *MIT Press*, 1972.

[24] Eleuterio Francisco Toro. *Riemann solvers and numerical methods for fluid dynamics*. Springer Berlin Heidelberg, 1997.

[25] Ziniu Wu, Yizhe Xu, Wenbin Wang, and Ruifeng Hu. Review of shock wave detection method in cfd post-processing. *Chinese Journal of Aeronautics*, 26(3):501–513, 2013.